electrochem

MDPI

Review

Crystal Structure and Preparation of $Li_7La_3Zr_2O_{12}$ (LLZO) Solid-State Electrolyte and Doping Impacts on the Conductivity: An Overview

Md Mozammal Raju [1], Fadhilah Altayran [1,2], Michael Johnson [1,2], Danling Wang [1,2] and Qifeng Zhang [1,2,*]

[1] Department of Electrical and Computer Engineering, North Dakota State University, Fargo, ND 58108, USA; mdmozammal.raju@ndsu.edu (M.M.R.); fadhilah.altayaran@ndus.edu (F.A.); michael.johnson.1@ndsu.edu (M.J.); danling.wang@ndsu.edu (D.W.)
[2] The Materials and Nanotechnology Program, North Dakota State University, Fargo, ND 58105, USA
* Correspondence: qifeng.zhang@ndsu.edu

Abstract: As an essential part of solid-state lithium-ion batteries, solid electrolytes are receiving increasing interest. Among all solid electrolytes, garnet-type $Li_7La_3Zr_2O_{12}$ (LLZO) has proven to be one of the most promising electrolytes because of its high ionic conductivity at room temperature, low activation energy, good chemical and electrochemical stability, and wide potential window. Since the first report of LLZO, extensive research has been done in both experimental investigations and theoretical simulations aiming to improve its performance and make LLZO a feasible solid electrolyte. These include developing different methods for the synthesis of LLZO, using different crucibles and different sintering temperatures to stabilize the crystal structure, and adopting different methods of cation doping to achieve more stable LLZO with a higher ionic conductivity and lower activation energy. It also includes intensive efforts made to reveal the mechanism of Li ion movement and understand its determination of the ionic conductivity of the material through molecular dynamic simulations. Nonetheless, more insightful study is expected in order to obtain LLZO with a higher ionic conductivity at room temperature and further improve chemical and electrochemical stability, while optimal multiple doping is thought to be a feasible and promising route. This review summarizes recent progress in the investigations of crystal structure and preparation of LLZO, and the impacts of doping on the lithium ionic conductivity of LLZO.

Keywords: LLZO; solid-state electrolyte; first-principles computing; synthesis; doping; lithium ionic conductivity

Citation: Raju, M.M.; Altayran, F.; Johnson, M.; Wang, D.; Zhang, Q. Crystal Structure and Preparation of $Li_7La_3Zr_2O_{12}$ (LLZO) Solid-State Electrolyte and Doping Impacts on the Conductivity: An Overview. *Electrochem* **2021**, 2, 390–414. https://doi.org/10.3390/electrochem2030026

Academic Editor: Masato Sone

Received: 20 April 2021
Accepted: 7 July 2021
Published: 19 July 2021

1. Introduction

Many countries around the world are setting up renewable energy plants, reducing the use of carbon emitting fuels, making electric vehicles (EV's), and taking many other initiatives to tackle the energy crisis that is imminent because of increasing burn rates of fossil fuels; and most of these initiatives need reliable energy storage devices which will ensure the efficient use of the said energy. Therefore, for now, the main challenge regarding effective use of energy is to make energy conversion and storage more efficient and more reliable.

Among many energy storage devices, lithium-ion battery has been the most commonly used technology because of its advantages including high energy density, long duty cycle, low self-discharge, and light weight [1–3]. However, there are some concerns about lithium-ion batteries like: safety issues because of the formation of dendrites, reduced power capability because of the formation of solid electrolyte interface (SEI) from continuous charging and discharging, low ionic conductivity, and high cost compared to other existing rechargeable batteries. Extensive research is being carried out by many groups to resolve these issues aiming to improve the performance of lithium-ion batteries.

Electrolyte is one of the most important parts that determine the performance of lithium-ion batteries. According to the state of form, electrolyte materials can be categorized as liquid electrolytes, polymer electrolytes, ionic electrolytes, and solid electrolytes.

Liquid electrolytes are made by dissolving various Li-rich salts like Li_3N, $LiPF_6$, $LiClO_4$, etc. into solvents. The main advantage of liquid electrolytes is the high ionic conductivity on the order of 10^{-2} S/cm, while the major problem of liquid electrolytes is that they react with electrodes creating a solid electrolyte interface (SEI) layer which lowers battery performance and increases safety concerns [4].

Polymer electrolytes (PE) are defined as a solvent-free salt solution in a polymer host material such as polyethylene oxide (PEO) that conducts lithium ions through the polymer chains. Polymer electrolytes typically have an ionic conductivity in the range of 10^{-4} to 10^{-8} S/cm [5,6]. The main advantage of polymer electrolytes is that they can form a very thin layer of electrolyte which exhibits a low internal resistance, thus delivering batteries with a high specific power density [7]. However, polymer electrolytes also react with Li electrode leading to the formation of a SEI layer at the interface between electrodes and electrolyte.

Ionic electrolytes are composed of organic salts such as alkylammonium, N-alkyl pyridinium, phosphonium, etc. [8,9]. They show very good electrochemical and thermal stability. Moreover, they are inflammable and recyclable. However, due to the high viscosity, ionic electrolytes usually present a poor ionic conductivity [10].

Solid electrolytes have many advantages such as good chemical stability with Li metal electrode, good thermal stability, high electrochemical voltage window (>5 V), economy, and environmental friendliness. They exhibit an ionic conductivity typically in the range of 10^{-3} to 10^{-7} S/cm, which is relatively lower than that of liquid electrolytes. Because solid electrolytes can be used to form all solid-state batteries (ASSBs), they have been intensively studied. Solid electrolytes can be categorized mainly into three types: inorganic solid electrolytes, solid polymer electrolytes and solid composite polymer electrolytes.

Research has been performed on various types of inorganic solid electrolyte: Li_3N type, [11–13] LISICON type, [14–16] NASICON type, [17–24] beta alumina type, [25–29] LIPON type, [30–32] and perovskite type; [33,34] but the problems with these types of inorganic electrolytes are: (1) poor chemical stability due to the reaction with metal electrodes, (2) difficulty to prepare, (3) a low electrochemical voltage window, and (4) low ionic conductivity.

In 2003, Thangadurai et al. first reported the use of inorganic garnet-type lithium oxide with a nominal composition of $Li_5La_{3\times 2}O_{12}$ (X = Nb, Ta) for ASSB and showed the promising capability in overcoming the problems mentioned above [35]. In 2007, the same group reported the most promising garnet-type Li oxide with nominal composition of $Li_7La_3Zr_2O_{12}$, also known as LLZO, which revealed excellent properties with exceptional results that exceeded all the previous findings of solid electrolytes [36]. Since its first report, LLZO has drawn great attention of the battery research community; in order to use in practical purpose application a considerable amount of research has been undertaken to increase the performance of LLZO.

In 2015, Ramakumar et al. reported that among all garnet-type electrolytes, LLZO with a composition of $Li_7La_3Zr_2O_{12}$ exhibits the highest ionic conductivity corresponding to the lowest activation energy [37]. At 33 °C, $Li_7La_3Zr_2O_{12}$ composition exhibited a total (bulk + grain boundary) ionic conductivity of 5×10^{-4} S/cm with an activation energy of 0.32 eV. However, with further increasing Li content, the total ionic conductivity starts to decrease; in the case of 7.5 molar unit of Li content, the conductivity drops to 1×10^{-4} S/cm with the activation energy increasing to 0.38 eV [37].

In this paper, we review different crystal structures of LLZO, various synthesis methods for the preparation of LLZO, the molecular dynamics in relation to Li ion diffusion in LLZO, and the effects of different cation dopants on the conductivity of LLZO. The paper starts with an introduction, followed by five sections on the topics of (i) structural analysis, (ii) synthesis techniques for LLZO, (iii) sintering techniques, (iv) Li ion diffusion

mechanism, and (v) doping and Li ionic conductivity, and ends with a conclusion section that summarizes the major conclusions and addresses the challenges of on-going LLZO research. The goal of this article is to outline the optimal crystal structure with a doping strategy that may guide the experimental synthesis towards improving the lithium ionic conductivity of LLZO solid electrolyte.

2. Structural Analysis of LLZO

In 2003, Thangadurai et al. reported $Li_5La_3M_2O_{12}$ (M = Nb, Ta) oxides as a fast garnet-like Li-ion conductor [35]. Later in 2007, from the same group Murugan et al. introduced a new garnet-type material $Li_7La_3Zr_2O_{12}$ known as LLZO which has higher ionic conductivity at room temperature [36]. The generic formula for LLZO garnet $Li_7La_3Zr_2O_{12}$ was derived from the garnet type family $Li_7A_3B_2O_{12}$, in which Li ions occupy octahedral and tetrahedral sites, A-cations belong to eight-coordination sites and B-cations belong to six-fold coordination sites. LLZO exhibits two phases, namely tetragonal phase (lattice parameter: a = b $\neq$ c, angle: $\alpha = \beta = \gamma = 90^\circ$, space group $I4_1/acd$) and cubic phase (lattice parameter: a = b = c, angle: $\alpha = \beta = \gamma = 90^\circ$, space group $Ia\bar{3}d$). Both phases possess the same structural framework but there is a difference in the distribution of Li atoms, which dominantly determines the ionic conductivity of LLZO. In the tetragonal phase, Li ions can occupy tetrahedral 8a, and octahedral 16f and 32g sites as shown in Figure 1, [38] where Li(1) is in 8a tetrahedral site connected to four O atoms; Li(2) and Li(3) belong to 16f and 32g octahedral sites, respectively, and both are connected to six O atoms. Unlike the tetragonal phase, Li in cubic structure occupies only 2 different sites namely 24d tetrahedral sites and 96h octahedral sites as shown in Figure 2 [39]. Therefore, it is clear from the site occupancy perspective that in the cubic phase Li ions have more available sites for migration than in the tetragonal phase.

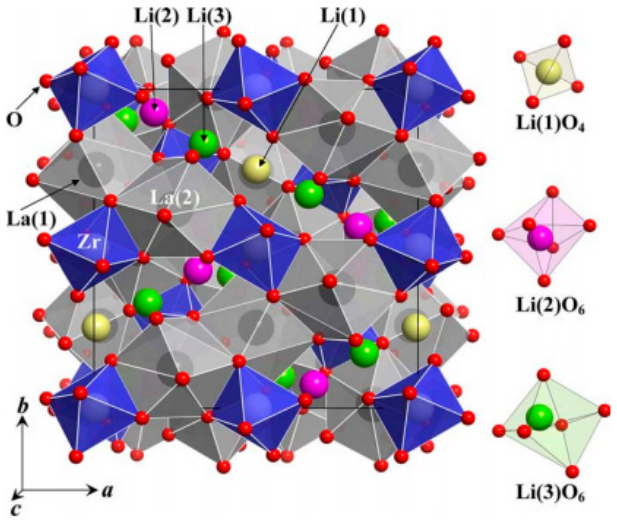

Figure 1. Crystal structure of a unit cell of 8 per formula unit (pfu) in tetragonal LLZO ($Li_7La_3Zr_2O_{12}$). Shown on right side are three different lithium sites: 8a, 16f and 32g (reprinted from [38]).

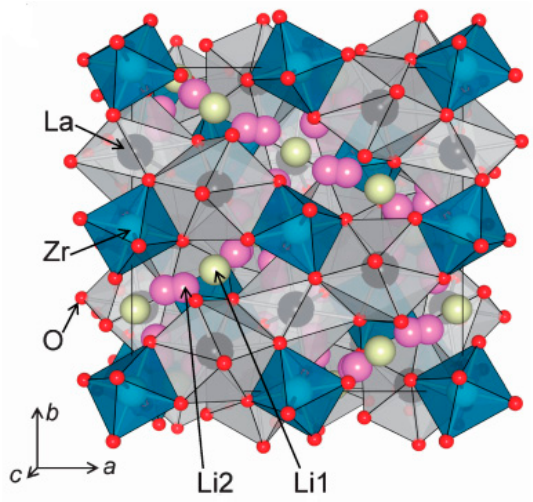

Figure 2. Crystal structure of a unit cell of 8 pfu cubic LLZO, where Li1 white spheres represent 24d tetrahedral sites and Li2 pink spheres represent 96h octahedral sites (reprinted from [39]).

Therefore, for an 8 per formula unit (pfu) LLZO cell which has 56 Li atoms, the total number of positions available for Li atoms in tetragonal phase is 56 (tetrahedral 8a, octahedral 16f and 32g), but in cubic phase the total number of positions available for Li atoms is 120 (tetrahedral 24d, octahedral 96h). In other words, in the cubic phase Li has 64 empty positions available for migration, but in the tetragonal phase all the positions (the sites 8a, 16f and 32g) are filled—and thus there is no vacancy for movement of Li as shown in Figure 3a [39]. According to Awaka et al., in cubic-phase LLZO the tetrahedral sites are more likely to be occupied than octahedral sites as shown in Figure 3b, where more vacant octahedral sites are available to be occupied [38]. Similar hypothesis has been given by Bernstein et al. [40] as shown in Figure 4, according to Bernstein the 8a sites which are filled in the tetragonal phase are identified as 24d in cubic phase are almost filled; while 16f and 32g sites which are full in the tetragonal phase are identified as 96h in the cubic phase which has more empty positions available (because of Coulomb repulsion) to be filled [40].

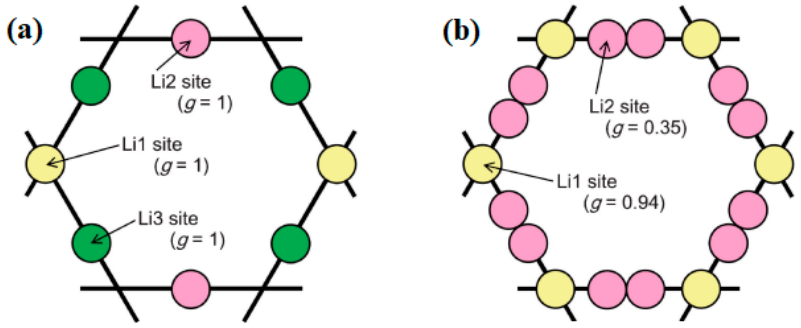

Figure 3. Loop structure of Li arrangement in (**a**) tetragonal phase where Li1, Li2 and Li3 represent 8a, 16f and 32g site, respectively, (**b**) cubic phase where Li1 and Li2 represent 24d and 96h site, respectively, and g denotes the occupancy for each site (reprinted from [39]).

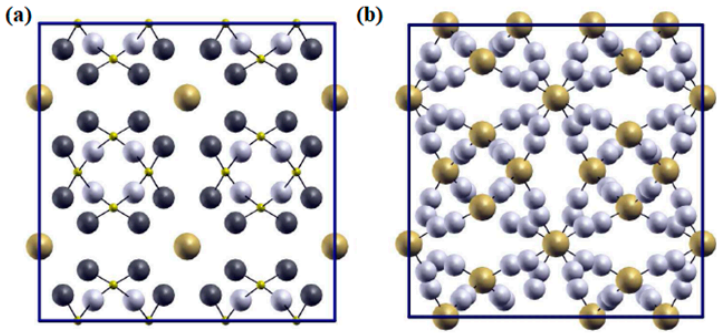

Figure 4. Two-dimensional view of (**a**) tetragonal phase where large gold, white and dark grey spheres represent 8a, 16f and 32g sites, respectively, and (**b**) cubic phase where all the possible 120 positions of Li are represented by gold and white spheres corresponding to 24d and 96h sites, respectively (reprinted from [40]).

Awaka and Bernstein suggested higher occupancy of tetrahedral sites than octahedral sites [39,40]; however, a simulated study done by Meier et al., using the first principles method with molecular metadynamics on CP2K, found the opposite scenario [41,42]. They took 120 randomly generated structures where 56 Li atom can fill 72 available sites (considering 48 octahedral sites because two neighboring octahedral sites cannot be occupied) obeying Coulomb repulsion; they found very interesting and convincing results which indicate that the cubic phase LLZO octahedral site has higher occupancy than the tetrahedral site. They have shown that the most stable structure is the structure that possesses the lowest potential energy, in which Li atoms occupy 11 out of 24 tetrahedral sites (about 46%) and 45 out of 48 octahedral sites (about 94%). Figure 5b indicates that the average occupancy of blue dots is about 60% whereas for red dots it is about 85%, which shows that tetrahedral sites have lower occupancy than octahedral sites [41].

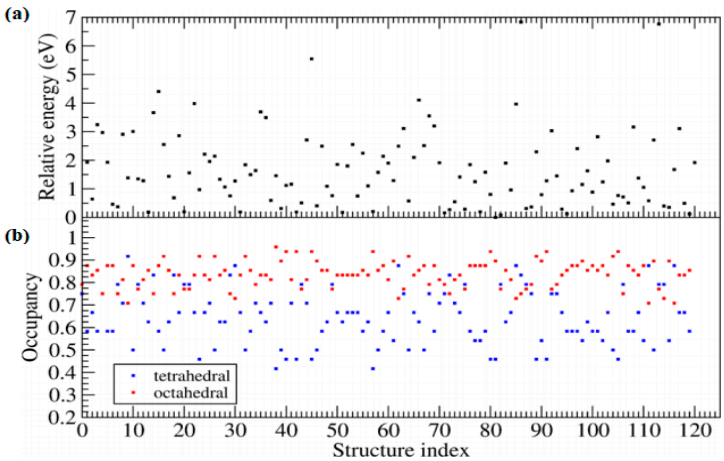

Figure 5. (**a**) Relative energy of 120 random cubic LLZO structures where number 81 has the lowest potential energy. (**b**) The occupancy of 120 random structures where blue and red dots indicate the occupancy of tetrahedral and octahedral sites, respectively (reprinted from [41]).

Transition to Cubic Phase from Tetragonal Phase and Vice Versa

Among the two phases of LLZO, the tetragonal phase shows good stability at room temperature but exhibits a low Li ionic conductivity, typically on the order of 10^{-6} S/cm; whereas at higher temperatures the tetragonal phase transforms into cubic phase which shows a higher Li ionic conductivity on the order of 10^{-4} S/cm, about 100 times that of the tetragonal phase. The transition temperature typically lies between 450–1000 K [36,38–40,43–48].

The crystal structure shown in Figure 6 reported by Cao et al. reveals that both tetrahedral and cubic phase LLZO have the same structural framework except in Li distribution [49]. Bernstein et al. reported that tetragonal phase LLZO presents good stability due to its ordered geometry. During the phase transformation, as shown in Figure 4a, the tetrahedral 8a site transforms into the tetrahedral 16e site and ultimately converts into tetrahedral 24d site, and octahedral 16f and 32g sites transform into octahedral 96h site in cubic LLZO [40]. Geiger et al. suggested that the ionic conductivity of cubic LLZO increases because of the decrease in distance between neighboring Li pairs [43]; but Meier et al. found no difference in neighboring Li–Li pair distance in their simulated study shown in Figure 7 [41].

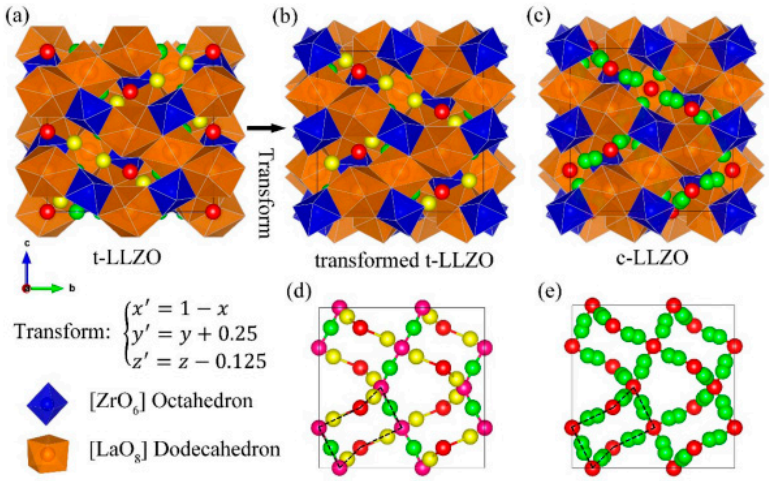

Figure 6. Crystal structure of (**a**) tetragonal phase, (**b**) transformed tetragonal phase, and (**c**) cubic phase LLZO where the blue and brown polyhedral indicates six- and eight-fold coordination sites, respectively. The distribution of Li in tetragonal phase (**d**), and in cubic phase (**e**). (reprinted from [49]).

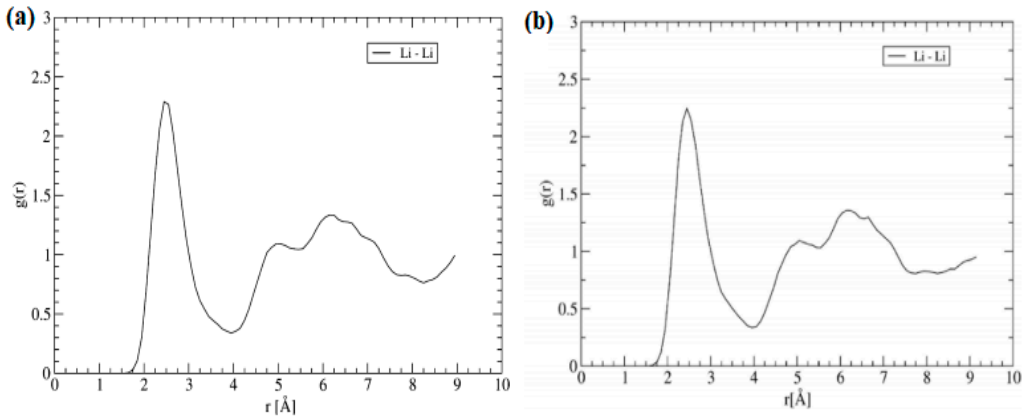

Figure 7. Radial distribution for Li-Li pairs over 20 ps ab-initio molecular dynamics simulated study for (**a**) tetragonal LLZO and (**b**) cubic LLZO (reprinted from [41]).

In 2015, Klenk and Lai reported the transformation of tetragonal phase into cubic phase using MD simulation. For tetragonal phase they used cage occupancy of four sites (8a, 16e, 16f and 32g) as a function of temperature, and mean squared displacement (MSD) as a function of time [46]. The results published by Klenk are in contrast to the observation revealed by Bernstein et al. [40], according to their observation with the increase in temperature the occupancy of site 8a decreases, and the occupancy of site 16e increases, but the change in octahedral sites 16f and 32g are very negligible, which indicates tetragonal sites 8a and 16e are exchanging Li atoms; but Bernstein et al. stated that there is no exchange

of Li atom between 8a and 16e. However, both groups reported the simultaneous increase in MSD of Li atoms of tetrahedral 8a sites and octahedral 32g sites, and pointed out that the change of positions of Li atoms at site 8a and 32g are correlated [40,46].

Using X-ray diffraction (XRD) patterns, Adams and Rao revealed the gradual transformation of tetragonal LLZO into cubic LLZO [48]. According to their report, at low temperature the LLZO shows tetragonal phase characteristic with two Bragg peaks at 211 and 112; but as the temperature increases the 211 peak becomes more pronounced whereas the 112 peak vanishes gradually, after 450 K the 112 peak disappears completely, which clearly indicates the transformation of tetragonal into cubic phase LLZO. Geiger et al. also mentioned, within the range of 400 K to 600 K, the tetragonal phase transforms into octahedral phase [43]. Adams and Rao investigated the transformation of doped LLZO, and interestingly found that the transformation can happen even at room temperature [48].

Mori et al. experimentally found that by adding Ga impurity into LLZO, it is possible to obtain cubic phase Ga-LLZO and it can be reversed into tetragonal phase by doping another elemental cation like Sr [50]. When the doping level of Sr reaches to a maximum limit the cubic phase of GaSr-LLZO transforms into tetragonal phase as shown in Figure 8a [50]. The XRD patterns of the samples at different proportions of Sr content reveal that up to 0.2 pfu the structure remains cubic, but further increase in Sr content converts the material into tetragonal phase, which is shown in the upper three XRD patterns corresponding to the samples which contain 0.3, 0.4 and 0.5 pfu of Sr, respectively. Figure 8b suggests that, with increasing Sr content, the volume of sample also increases linearly up to 0.125 pfu, and then turns to a platform in the range from 0.125–0.2 pfu. With further increasing Sr content above a molar value of 0.2, the lattice parameter increases discontinuously due to a change in the crystal phase from cubic to tetragonal. A similar tendency was reported elsewhere [51–53].

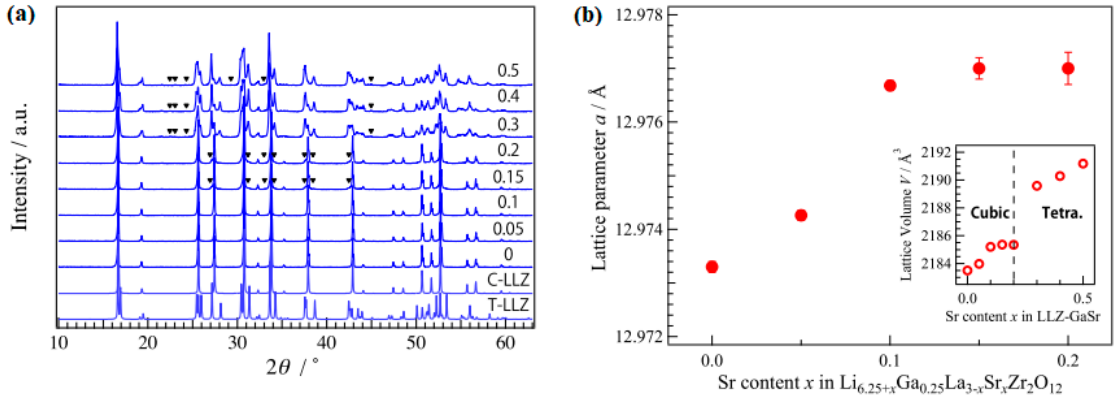

Figure 8. (**a**) X-ray diffraction (XRD) patterns of GaSr-LLZO that contains various content of Sr where the bottom two T-LLZ and C-LLZ represents simulated pattern of tetragonal and octahedral phase respectively for comparison, and (**b**) the change in volume with the change in Sr content, the volumetric change from cubic phase to tetragonal phase with the increase in Sr content is shown (inset) (reprinted from [50]).

3. Synthesis Techniques of LLZO ($Li_7La_3Zr_2O_{12}$)

Pure and doped LLZO can be prepared in many ways, such as the solid-state reaction, sol-gel method, Pechini method, RF magnetron sputtering method, and pulsed laser deposition method.

3.1. Solid-State Reaction Method

Solid-state reactions are a commonly used technique which involve ball milling, grinding, and sintering of the precursor material to get the final solid electrolyte material. In this process the preliminary grinding is generally performed using a ball mill or a planetary milling machine, the output of ground powder may be wet, which is then dried

and sintered or annealed at high temperature in a furnace. This process of grinding and sintering needs to be repeated as the first sequence of grinding and sintering is employed to mix the precursor contents and the subsequent grinding along with sintering is repeated to produce a finer and denser particle. Finally, the precursor powder is pelletized using a hydraulic press and then sintered again at elevated temperature to obtain a more compact and non-porous solid electrolyte. This process is preferred because of its low cost, simplicity, and high throughput.

The first LLZO was prepared by Murugan et al. in 2007 using solid state reaction technique where they used sintering temperature of 1230 °C for 36 h [36]. After 2007 this became the most widely used method; however, some researchers reported some concerns regarding this process: (1) the method is difficult in achieving desired stoichiometric structure, (2) high sintering temperature introduces impure phases into the system, (3) the long period of high sintering processing causes too much Li loss from the system, and (4) at high temperature, other foreign elements are introduced from the crucible containing the sample [54,55].

3.2. Sol-Gel Method

To avoid the problems arising from high sintering temperatures during solid state reaction, which causes Li loss and creates impure phase formation in the system, the sol-gel method has been developed which involves hydrolysis and polymerization. The sol-gel method uses relatively low temperatures and yields uniformly distributed finer sized particles without needing intermittent grinding [56].

$Li_5La_3Ta_2O_{12}$ garnet was first prepared using the sol-gel method by Gao et al. [57] Kokal et al. and Shimonishi et al. reported the preparation of cubic LLZO using the sol-gel technique followed by sintering at the temperatures of 700 °C and 1180 °C, respectively [58,59]. However, Li garnets obtained through sol-gel shows a relatively low ionic conductivity [59,60]. In 2014, Janani et al. introduced a new sol-gel technique which uses additives during the sintering process, yielding Al-doped LLZO with an improved ionic conductivity of 6.1×10^{-4} S/cm at 33 °C and relative density of 96% [61].

3.3. Pechini Method

The Pechini method is a modified technique of the sol-gel method which involves the ability to chelate metal ions with the help of carboxylic acids such as tartaric acid, citric acid, etc. and forms a polymeric resin due to polysensitization when heated with polyethylene glycol or another hydroxylic alcohol agent. This process requires lower sintering temperature, shorter reaction time and yields uniformly distributed nanosized particles. Using the Pechini method, Gao et al. synthesized $Li_5La_3Bi_2O_{12}$ nanocrystalline powder [62], and Jin et al. synthesized stable cubic Al-doped LLZO [63].

3.4. Radio Frequency (RF) Magnetron Sputtering

Radio frequency (RF) magnetron sputtering is a thin film processing technique in which a thin layer of LLZO layer is deposited through RF-powered sputtering. The main advantage of this established process is ease of control. In 2016, RF magnetron sputtering was used by Lobe et al. to prepare thin film cubic LLZO with a substrate temperature of 700 °C [64]. (Earlier in 2012, Kalita et al. reported the successful deposition of amorphous thin film LLZO using the RF sputtering technique [65].) However, it came with limited yield capability and meanwhile the resulted ionic conductivity is poor.

3.5. Pulsed Laser Deposition

Pulsed laser deposition (PLD) has also been used for the fabrication of LLZO. In PLD, a laser beam usually ablates the targets at a suitable angle which helps to preserve the stoichiometry and composition of the target. PLD is very flexible process as it allows the adjustment of conditions that are appropriate for deposition such as the energy of laser density, temperature, and pressure. Also, it reduces the Li loss that occurs during the

synthesis process as it allows films to be grown at low temperature in a shorter period. However, a very few studies have been reported so far that used PLD for LLZO preparation. The effect of different substrates on the growth of LLZO at different deposition temperature were investigated by Park et al. [66]. Tan et al. used this method to prepare LLZO on sapphire and $SrTiO_3$ substrates [67].

Table 1 outlines the Li ionic conductivity and the activation energy reported by different research groups where they used different synthesis techniques. Besides the methods discussed above and listed in Table 1, there are also some other methods which have been adopted to prepare solid-state LLZO, such as epitaxial growth [68], combustion method [69,70], sol-gel spin coating [71,72] and nebulized spray pyrolysis [73].

Table 1. The sintering temperature, space group, Li ionic conductivity (σ) and total activation energy (E_a) of pure and doped LLZO prepared by various research group using different synthesis processes.

Chemical Composition	Year Reported	Synthesis Process	Space Group	Ionic Conductivity, σ (mS/cm)	Activation Energy, E_a (eV)	σ_{total} Measuring Temperature (°C)	Ref.
$Li_7La_3ZrNb_{0.5}Y_{0.5}O_{12}$	2018	SSR	$Ia\bar{3}d$	0.830 (T)	0.31	30	[74]
$Li_{6.4}Fe_{0.2}La_3Zr_2O_{12}$	2018	SSR	$Ia\bar{3}d$	1.100 (T)	-	RT	[75]
$Li_{6.25}Ga_{0.25}La_3Zr_2O_{12}$	2017	SSR	$Ia\bar{3}d$	1.460 (T)	0.25	RT	[76]
$Li_7La_3Zr_2O_{12}$	2015	SSR	$Ia\bar{3}d$	0.174 (B)	0.26 (Bulk)	25	[77]
$Li_{6.4}La_3Zr_{1.4}Ta_{0.3}Nb_{0.3}O_{12}$	2015	SSR	$Ia\bar{3}d$	0.606 (B)	0.26 (Bulk)	25	[77]
$Li_{6.4}La_3Zr_{1.4}Ta_{0.4}Nb_{0.2}O_{12}$	2015	SSR	$Ia\bar{3}d$	0.455 (B)	0.28 (Bulk)	25	[77]
$Li_{6.4}La_3Zr_{1.4}Ta_{0.5}Nb_{0.1}O_{12}$	2015	SSR	$Ia\bar{3}d$	0.444 (B)	0.27 (Bulk)	25	[77]
$Li_{6.4}La_3Zr_{1.4}Ta_{0.6}O_{12}$	2015	SSR	$Ia\bar{3}d$	0.724 (B)	0.24 (Bulk)	25	[77]
$Li_{6.65}La_{2.75}Ba_{0.25}Zr_{1.4}Ta_{0.5}Nb_{0.1}O_{12}$	2015	SSR	$Ia\bar{3}d$	0.527 (B)	0.26 (Bulk)	25	[77]
0.5F-LLZO	2015	SSR	$Ia\bar{3}d$	0.450 (T)	-	RT	[78]
1.0F-LLZO	2015	SSR	$Ia\bar{3}d$	0.500 (T)	0.26	RT	[78]
1.5CF-LLZO	2015	SSR	$Ia\bar{3}d$	0.050 (T)	-	RT	[78]
2.0Al-LLZO	2015	SSR	$Ia\bar{3}d$	0.200 (T)	-	RT	[78]
$Li_7La_3Zr_2O_{12}$	2015	SSR	$I4_1/acd$	0.017 (T)	0.47	25	[79]
$Li_{5.9}La_3Zr_{1.45}W_{0.55}O_{12}$	2015	SSR	$Ia\bar{3}d$	0.440 (T)	0.43	25	[79]
$Li_{6.5}La_3Zr_{1.75}W_{0.25}O_{12}$	2015	SSR	$Ia\bar{3}d$	0.490 (T)	0.42	25	[79]
$Li_{6.30}La_3Zr_{1.65}W_{0.35}O_{12}$	2015	SSR	$Ia\bar{3}d$	0.660 (T)	0.42	25	[79]
$Li_{6.1}La_3Zr_{1.55}W_{0.45}O_{12}$	2015	SSR	$Ia\bar{3}d$	0.640 (T)	0.43		[79]
$Li_6La_3Ta_{1.5}Y_{0.50}O_{12}$	2015	SSR	$Ia\bar{3}d$	0.126 (T)	0.37	23	[80]
$Li_{6.5}La_3Ta_{1.25}Y_{0.75}O_{12}$	2015	SSR	$Ia\bar{3}d$	0.183 (T)	0.33	23	[80]
$Li_{6.25}La_3Nb_{1.375}Sc_{0.625}O_{12}$	2015	SSR	$Ia\bar{3}d$	0.102 (T)	0.48	25	[81]
$Li_{6.25}La_3Nb_{0.75}Zr_{1.25}O_{12}$	2015	SSR	$Ia\bar{3}d$	0.203 (T)	0.42	25	[81]
$Li_{6.5}La_{1.5}Ba_{1.5}Ta_2O_{12}$	2015	SSR	$Ia\bar{3}d$	0.062 (T)	0.40	33	[37]
$Li_{6.28}Al_{0.24}La_3Zr_2O_{12}$	2015	SSR	$Ia\bar{3}d$	0.443 (T)	0.37	30	[82]
$Li_{6.2}La_3Zr_{1.2}Ta_{0.8}O_{12}$	2015	SSR	$Ia\bar{3}d$	2.3×10^{-3} (T)	0.53	33	[83]
$Li_{5.5}La_3Zr_{1.25}W_{0.75}O_{12}$	2015	SSR	$Ia\bar{3}d$	0.053 (T)	0.43	25	[84]
$Li_7La_3Zr_2O_{12}$	2014	SSR	$I4_1/acd$	9.90×10^{-3} (T)	0.43	27	[85]
$Li_{6.75}La_3Zr_{1.75}Ta_{0.25}O_{12}$	2014	SSR	$Ia\bar{3}d$	0.410 (T)	0.42	27	[85]
$Li_{6.5}La_3Zr_{1.5}Ta_{0.5}O_{12}$	2014	SSR	$Ia\bar{3}d$	0.610 (T)	0.40	27	[85]
$Li_6La_3ZrTaO_{12}$	2014	SSR	$Ia\bar{3}d$	0.210 (T)	0.42	27	[85]
$Li_{6.925}La_3Zr_{1.925}Sb_{0.075}O_{12}$	2014	SSR	$Ia\bar{3}d$	0.340 (T)	0.37	30	[86]
$Li_7La_3Zr_2O_{12}$	2014	SSR	$Ia\bar{3}d$	0.120 (T)	0.41	30	[86]
$Li_7La_3Nb_2ScO_{12}$	2014	SSR	$Ia\bar{3}d$	0.068 (T)	0.40	25	[87]
$Li_6La_3Nb_{1.5}Sc_{0.5}O_{12}$	2014	SSR	$Ia\bar{3}d$	0.102 (T)	0.40	25	[87]
$Li_{6.25}La_3Nb_{1.375}Sc_{0.625}O_{12}$	2014	SSR	$Ia\bar{3}d$	0.138 (T)	0.36	25	[87]
$Li_{6.5}La_3Nb_{1.25}Sc_{0.75}O_{12}$	2014	SSR	$Ia\bar{3}d$	0.126 (T)	0.39	25	[87]
$Li_5La_3Nb_2O_{12}$	2014	SSR	$Ia\bar{3}d$	0.022 (T)	0.45	25	[87]
$Li_{5.5}La_3Nb_{1.75}Sc_{0.25}O_{12}$	2014	SSR	$Ia\bar{3}d$	0.052 (T)	0.40	25	[87]
$Li_{6.5}La_3Ta_{1.25}Y_{0.75}O_{12}$	2014	SSR	$Ia\bar{3}d$	0.183 (T)	0.36	23	[88]
$Li_{6.75}La_3Zr_{1.75}Ta_{0.25}O_{12}$ with flow of O_2	2014	SSR	$Ia\bar{3}d$	0.740 (T)	0.33	25	[89]
$Li_{6.75}La_3Zr_{1.75}Ta_{0.25}O_{12}$ with flow of Air	2014	SSR	$Ia\bar{3}d$	0.240 (T)	0.39	25	[89]
$Li_{6.5}La_3Ta_{0.5}Zr_{1.5}O_{12}$ 30 mol.% excess Li	2014	SSR	$Ia\bar{3}d$	0.433 (T)	-	RT	[54]
$Li_6La_3Zr_{1.5}Te_{0.5}O_{12}$	2014	SSR	$Ia\bar{3}d$	2.19×10^{-3} (T)	0.37	RT	[90]
$Li_6Ba_{0.5}Sr_{0.5}La_2Ta_2O_{12}$	2014	SSR	$Ia\bar{3}d$	7.19×10^{-3} (T)	0.45	18	[91]
$Li_7La_3Zr_2O_{12}$	2013	SSR	$I4_1/acd$	5.77×10^{-3} (T)	0.40	RT	[92]
$Li_{6.6}La_{2.6}Ce_{0.4}Zr_2O_{12}$	2013	SSR	$Ia\bar{3}d$	0.0144 (T)	0.48	RT	[92]
$Li_{6.4}La_{2.4}Ce_{0.6}Zr_2O_{12}$	2013	SSR	$Ia\bar{3}d$	0.0126 (T)	0.50	RT	[92]
$Li_{7.06}La_3Zr_{1.94}Y_{0.06}O_{12}$	2013	SSR	$Ia\bar{3}d$	1.0×10^{-3} (B)	0.47	23	[93]
$Li_{7.16}La_3Zr_{1.84}Y_{0.16}O_{12}$	2013	SSR	$Ia\bar{3}d$	1.0×10^{-3} (B)	0.47	23	[93]
$Li_7Nd_3Zr_2O_{12}$	2013	SSR	$I4_1/acd$	-	0.66	-	[94]
$Li_7La_3Zr_2O_{12}$	2013	SSR	$Ia\bar{3}d$	0.500 (T)	0.31	24	[51]
$Li_6BaLa_2Ta_2O_{12}$	2013	SSR	$Ia\bar{3}d$	0.10 (T)	0.39	25	[95]
$Li_7La_3Ta_2O_{13}$	2013	SSR	$Ia\bar{3}d$	3.21×10^{-3} (B)	0.55	40	[96]
$Li_{6.75}La_3Zr_{1.75}Ta_{0.25}O_{12}$	2013	SSR	$Ia\bar{3}d$	0.640 (T)	0.30	28	[97]
$Li_{6.75}La_3Zr_{1.875}Te_{0.125}O_{12}$	2013	SSR	$Ia\bar{3}d$	0.330 (T)	0.41	30	[98]

Table 1. *Cont.*

Chemical Composition	Year Reported	Synthesis Process	Space Group	Ionic Conductivity, σ (mS/cm)	Activation Energy, E_a (eV)	σ_{total} Measuring Temperature (°C)	Ref.
$Li_{6.6}La_3Zr_{1.6}Sb_{0.4}O_{12}$	2013	SSR	$Ia\bar{3}d$	0.770 (T)	0.34	30	[99]
$Li_{6.4}La_3Zr_{1.6}W_{0.3}O_{12}$	2013	SSR	$Ia\bar{3}d$	0.789 (T)	0.45	30	[100]
0.28Al-$Li_7La_3Zr_2O_{12}$	2012	SSR	$Ia\bar{3}d$	0.350 (T)	0.36	25	[101]
$Li_6La_3ZrTaO_{12}$	2012	SSR	$Ia\bar{3}d$	0.260 (T)	0.46	25	[101]
$Li_{6.5}La_3Zr_{1.5}Ta_{0.5}O_{12}$	2012	SSR	$Ia\bar{3}d$	2.0×10^{-3} (T)	0.49	25	[101]
$Li_{6.625}La_3Zr_{1.625}Ta_{0.375}O_{12}$	2012	SSR	$Ia\bar{3}d$	0.520 (T)	0.41	25	[101]
$Li_7La_3Zr_2O_{12}$	2012	SSR	$I4_1/acd$	1.3×10^{-3} (B)	0.46	20	[102]
0.204Al-$Li_7La_3Zr_2O_{12}$	2012	SSR	$Ia\bar{3}d$	0.400 (T)	0.26	RT	[55]
$Li_7La_3Zr_2O_{12}$	2012	SSR	$Ia\bar{3}d$	0.160 (T)	-	RT	[103]
Ge-$Li_7La_3Zr_2O_{12}$	2012	SSR	$Ia\bar{3}d$	0.763 (T)	-	25	[104]
$Li_{6.7}La_3Zr_{1.7}Ta_{0.3}O_{12}$	2012	SSR	$Ia\bar{3}d$	0.690 (T)	0.36	RT	[105]
$Li_{6.4}La_3Zr_{1.4}Ta_{0.6}O_{12}$	2012	SSR	$Ia\bar{3}d$	1.0 (T)	0.35	25	[106]
$Li_{6.5}La_{2.5}Ba_{0.5}ZrTaO_{12}$	2012	SSR	$Ia\bar{3}d$	0.090 (T)	0.57	24	[107]
$Li_7La_3Zr_2O_{12}$	2011	SSR	$I4_1/acd$	2.0×10^{-3} (T)	0.49	25	[47]
$Li_7La_3Zr_2O_{12}$	2011	SSR	$Ia\bar{3}d$	0.400 (T)	0.34	25	[47]
$Li_{7.06}La_3Y_{0.06}Zr_{1.94}O_{12}$	2011	SSR	$Ia\bar{3}d$	0.810 (T)	0.26	25	[108]
$Li_{6.75}La_3Zr_{1.75}Nb_{0.25}O_{12}$	2011	SSR	$Ia\bar{3}d$	0.80 (T)	0.31	25	[109]
$Li_6La_3ZrTaO_{12}$	2011	SSR	$Ia\bar{3}d$	0.180 (T)	0.42	25	[110]
$Li_7La_3Zr_2O_{12}$	2010	SSR	$Ia\bar{3}d$	0.180 (B)	-	25	[111]
$Li_7La_3Hf_2O_{12}$	2010	SSR	$Ia\bar{3}d$	0.240 (B)	0.29	25	[112]
$Li_7La_3Hf_2O_{12}$	2010	SSR	$I4_1/acd$	9.85×10^{-4} (B)	0.59	27	[113]
$Li_7La_3Ta_2O_{12}$	2009	SSR	$Ia\bar{3}d$	2.2×10^{-3} (T)	0.38	27	[114]
$Li_7La_3Zr_2O_{12}$	2009	SSR	$I4_1/acd$	1.63×10^{-3} (T)	0.54	27	[38]
$Li_7BaLa_2Ta_2O_{12.5}$	2008	SSR	$Ia\bar{3}d$	0.097 (T)	0.45	50	[115]
$Li_5BaLa_2Ta_2O_{11.5}$	2008	SSR	$Ia\bar{3}d$	4.9×10^{-3} (T)	0.51	50	[115]
$Li_{5.5}BaLa_2Ta_2O_{11.75}$	2008	SSR	$Ia\bar{3}d$	0.031 (T)	0.47	50	[115]
$Li_{5.75}BaLa_2Ta_2O_{11.875}$	2008	SSR	$Ia\bar{3}d$	0.089 (T)	0.44	50	[115]
$Li_7La_3Zr_2O_{12}$	2007	SSR	$Ia\bar{3}d$	0.774 (T)	0.30	25	[36]
$Li_7La_3Zr_2O_{12}$	2016	Sol-gel	$Ia\bar{3}d$	0.140 (T)	-	RT	[116]
$Li_{6.4}Ga_{0.2}La_3Zr_2O_{12}$	2015	Sol-gel	$Ia\bar{3}d$	0.024 (T)	0.32	RT	[69]
$Li_{6.16}Al_{0.28}La_3Zr_2O_{12}$	2014	Sol-gel	$I4_1/acd$	3.0×10^{-4} (T)	-	33	[61]
$Li_{6.16}Al_{0.28}La_3Zr_2O_{12}$	2014	Sol-gel	$Ia\bar{3}d$	0.110 (T)	0.38	33	[61]
$Li_7La_3Zr_2O_{12}$	2013	Sol-gel	$Ia\bar{3}d$	0.400 (T)	0.41	RT	[117]
$Li_7La_3Zr_{1.89}Al_{0.15}O_{12}$	2013	Sol-gel	$Ia\bar{3}d$	0.340 (T)	0.33	RT	[118]
$Li_6La_3Zr_2O_{11.5}$	2011	Sol-gel	$Ia\bar{3}d$	0.139 (T)	-	25	[59]
$Li_7La_3Zr_2O_{12}$	2011	Sol-gel	$Ia\bar{3}d$	-	-	-	[119]
$Li_5La_3Ta_2O_{12}$	2010	Sol-gel	$Ia\bar{3}d$	1.54×10^{-3} (T)	0.57	25	[57]
Al-$Li_7La_3Zr_2O_{12}$	2011	Pechini	$Ia\bar{3}d$	0.200 (T)	-	25	[63]
$Li_7La_3Zr_2O_{12}$	2011	Sol-gel and Pechini	$Ia\bar{3}d$	-	-	-	[58]
$Li_7La_3Zr_2O_{12}$	2011	Sol-gel and Pechini	$I4_1/acd$	3.12×10^{-4} (T)	0.67	25	[58]
$Li_5La_3Bi_2O_{12}$	2010	Pechini	$Ia\bar{3}d$	0.024 (T)	0.40	26	[62]
Al-LLZO	2016	RFMS	$Ia\bar{3}d$	0.120 (T)	0.47	25	[64]
$Li_7La_3Zr_2O_{12}$	2012	RFMS	$I4_1/acd$	4.0×10^{-4} (T)	0.70	25	[65]
$Li_7La_3Zr_2O_{12}$	2013	PLD	$Ia\bar{3}d$	2.50×10^{-3} (T)	0.52	25	[68]
$Li_7La_3Zr_2O_{12}$	2013	PLD	$Ia\bar{3}d$	0.010 (T)	0.55	25	[68]
Laser annealed $Li_7La_3Zr_2O_{12}$	2012	PLD	$I4_1/acd$	7.36×10^{-4} (T)	0.32	RT	[67]
Deposited on As $Li_7La_3Zr_2O_{12}$	2012	PLD	$I4_1/acd$	3.35×10^{-4} (T)	0.36	RT	[67]
Annealed at 800 °C $Li_7La_3Zr_2O_{12}$	2012	PLD	$I4_1/acd$	1.78×10^{-4} (T)	0.41	RT	[67]

SSR—Solid-state reaction, (T)—Total ionic conductivity (Bulk + Grain boundary), (B)-Bulk conductivity, RT—Room temperature, RFMS—Radio frequency magnetron sputtering, PLD—Pulsed laser deposition.

4. Sintering Techniques of LLZO

Sintering is one of the most important steps during the fabrication of solid-state electrolytes as it plays a vital role in densifying the pellet of electrolyte. Dense pellets have many advantages such as: (1) decreasing grain boundary resistance and thus decreasing the activation energy to increase the Li ionic conductivity, (2) suppressing the formation of dendrites and accordingly increasing the safe operation of the battery, and (3) increasing the mechanical strength of the battery. Being not dense enough or possessing high porosity in the solid electrolyte increases the chance of fragility, and hence may cause mechanical failure of the device. There are some techniques like furnace sintering [36], hot pressing [55], field assisted sintering technology (FAST) [120] and spark plasma sintering (SPS) [121] reported in the literature that can be used to improve the density of pellets.

4.1. Furnace Sintering

Furnace sintering is mostly used in conventional solid-state reaction methods, where a crucible loaded with the powder of mixed raw materials is heated at elevated temperatures in vacuum or in the presence of flowing oxygen, air, other gas, or any other agent for a certain period. Different combinations of approach in which optimal parameters are used to make fine and distributed particles that yield a denser pellet with a high Li ionic conductivity have been reported [36,58,59,117]. Table 2 summarizes the sintering temperatures and times used in synthesizing differently doped LLZO and the resultant Li ionic conductivity.

Table 2. Temperature and time duration used in high temperature sintering.

Chemical Composition	Sintering Temperature (°C)	Sintering Duration (Hours)	Total Li Ionic Conductivity (mS/cm) at (Temperature)	Reference
$Li_7La_3ZrNb_{0.5}Y_{0.5}O_{12}$	1230	15	0.830 (30 °C)	[74]
$Li_7La_3Zr_2O_{12}$	1230	36	0.30 (RT)	[36]
$Li_{6.75}La_3Zr_{1.75}Ta_{0.25}O_{12}$ (0 wt.% Li2O)	1230	6	0.220 (28 °C)	[97]
$Li_7La_3Zr_2O_{12}$ (1.7 wt.% Al + 0.1 wt.% Si)	1230	36	0.680 (25 °C)	[122]
$Li_7La_3Zr_2O_{12}$ (1.3 wt.% Al)	1230	36	0.240 (25 °C)	[122]
$Li_{6.75}La_3Zr_{1.75}Ta_{0.25}O_{12}$ (4 wt.% Li2O)	1200	6	0.440 (28 °C)	[97]
Al-$Li_7La_3Zr_2O_{12}$	1200	36	0.014 (RT)	[123]
Al-$Li_7La_3Zr_2O_{12}$	1200	6	0.020 (RT)	[63]
$Li_{6.75}La_3Zr_{1.75}Nb_{0.25}O_{12}$	1200	36	0.80 (RT)	[109]
$Li_6La_3Zr_2O_{11.5}$	1180	32	0.0140 (RT)	[59]
$Li_{6.75}La_3Zr_{1.75}Ta_{0.25}O_{12}$ (1 wt.% Li3PO4)	1175	6	0.720 (25 °C)	[124]
$Li_{6.75}La_3Zr_{1.75}Ta_{0.25}O_{12}$ (6 wt.% Li2O)	1170	6	0.640 (28 °C)	[97]
$Li_{5.9}Al_{0.2}La_3Zr_{1.75}W_{0.25}O_{12}$	1150	12	0.490 (RT)	[84]
$Li_7La_3Zr_{1.89}Al_{0.15}O_{12}$	1150	1	0.0340 (RT)	[118]
$Li_{6.75}La_3Zr_{1.75}Ta_{0.25}O_{12}$ (in Oxygen)	1140	9	0.740 (25 °C)	[89]
$Li_{6.75}La_3Zr_{1.75}Ta_{0.25}O_{12}$ (in Air)	1140	9	0.240 (25 °C)	[89]
$Li_{6.75}La_3Zr_{1.75}Ta_{0.25}O_{12}$ (in Nitrogen)	1140	9	0.210 (25 °C)	[89]
$Li_{6.75}La_3Zr_{1.75}Ta_{0.25}O_{12}$ (in Argon)	1140	9	0.180 (25 °C)	[89]
$Li_{6.4}La_3Zr_{1.75}Ta_{0.6}O_{12}$	1140	16	1.00 (RT)	[106]
$Li_7La_3Zr_2O_{12}$	1100	5	0.0140 (RT)	[116]
$Li_{6.42}Al_{0.32}La_3Zr_{1.91}O_{12.02}$	1000	7	0.0015 (RT)	[125]
$Li_7La_3Zr_2O_{12}$	1000	4	0.040 (RT)	[117]
Al-$Li_7La_3Zr_2O_{12}$	900	5	0.0019 (RT)	[126]
$Li_7La_3Zr_2O_{12}$	900	5	0.0003 (RT)	[58]

In 2013, Li et al. measured the relative density and the ionic conductivity of Ta-doped LLZO after 9 h of sintering at 1140 °C using different atmospheres including oxygen, air, nitrogen and argon [89]. They found that the relative densities of the pellets prepared under these atmospheres were about 96%, 93%, 91% and 90%, respectively. Figure 9 shows the SEM images of samples sintered at different atmospheres. It can be clearly seen that the use of oxygen as an environment yields the densest pellets with a big grain size and small grain boundary (Figure 9a), whereas the use of argon results in the least dense pellets with a relatively small grain size and large porosity (Figure 9d) [89].

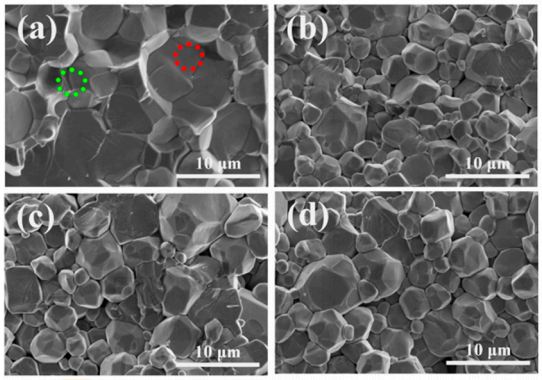

Figure 9. SEM images of Ta doped LLZO sintered at 1140 °C for 9 h in the atmospheres of (**a**) Oxygen, (**b**) Air, (**c**) Nitrogen and (**d**) Argon, where red and green circles in (**a**) indicate grain and intragrain boundary regions, respectively. (reprinted from [89]).

4.2. Hot Pressing

Hot pressing involves heat and pressure, where samples are sintered at high temperatures under a certain pressure. Simultaneous application of high temperature and pressure used in this process helps to stabilize the structure and densifies the pellets better. This method is also known as hot isostatic pressing (HIP). Table 3 shows the sintering temperature used in hot pressing by different groups for different doped LLZO along with the final sintering time duration, total Li ionic conductivity and relative density. It is evident that the pellets prepared in this process yield a much higher ionic conductivity. However, to obtain dense pellets, this method requires a significant amount of time for sintering.

Table 3. Relative density and ionic conductivity reported by researchers used hot isostatic pressing (HIP).

Chemical Composition	Sintering Temperature (°C)	Sintering Duration (Hours)	Total Li Ionic Conductivity (mS/cm) at (Temperature)	Relative Density in %	Reference
Al_2O_3-doped $Li_7La_3Zr_2O_{12}$	1180	127	0.990 (25 °C)	99.1	[127]
$Li_{6.55}Ga_{0.15}La_3Zr_2O_{12}$	1160	120	1.130 (25 °C)	97.5	[128]
$Li_{6.6}La_{2.6}Ce_{0.4}Zr_2O_{12}$	1050	40	0.014	96.0	[92]
$Li_{6.24}La_3Zr_2Al_{0.24}O_{11.98}$	1000	-	-	97.0	[129]
$Li_{6.25}La_3Zr_2Ga_{0.25}O_{12}$	1000	40	0.350 (RT)	91.0	[130]
$Li_{6.24}La_3Zr_2Al_{0.24}O_{11.98}$	1000	40	0.400 (RT)	98.0	[55]

4.3. Field-Assisted Sintering Technology (FAST)

Field-assisted sintering technology (FAST) is a sophisticated modern technology used to sinter samples at a high heating rate. The process of FAST is similar to that of hot isostatic pressing (HIP), however, a dc current passes through the tool along with the uniaxial pressure to assist in sintering process. In other words, the additional heat is generated by an external electrical circuit. FAST has many advantages over other sintering methods in terms of the fast-sintering process that saves time and reduction in Li ion loss that usually occurs due to a long sintering duration. As the synthesis of raw materials and sintering are done together at one time, it avoids the process of tedious intermittent

grinding and repeated long-time sintering. Table 4 shows the sintering temperature used in FAST by different researcher groups for various doped LLZO along with the sintering time duration, total Li ionic conductivity and relative density. In comparison to furnace sintering method, FAST can yield much denser Al-doped LLZO pellets with a higher ionic conductivity at room temperature.

Table 4. Relative density and ionic conductivity reported by researchers using the field-assisted sintering technology (FAST) method.

Chemical Composition	Sintering Temperature (°C)	Sintering Duration (Hours)	Total Li Ionic Conductivity (mS/cm) at (Temperature)	Relative Density in %	Reference
Al doped LLZO	1150	10	0.570 (RT)	99.8	[120]
Al doped LLZO	1000	10	0.332 (RT)	96.5	[131]
$Li_{6.49}La_3Zr_2Al_{0.17}O_{12}$	950	50	0.330 (25 °C)	96.0	[132]
Al doped LLZO	900	10	0.034 (RT)	88.9	[131]

4.4. Spark Plasma Sintering (SPS)

Spark plasma sintering (SPS) is similar to FAST except the use of pulsed direct current (DC). SPS uses a high current to create spark plasma between the sample particles; then the sample is compressed uniaxially for densification. SPS also has the advantages of reducing Li loss, making fine and distributed nanosized particles, and reducing boundary resistance. Table 5 shows the sintering temperature used in SPS for Ta/Ti doped LLZO along with the sintering time duration and total Li ionic conductivity with relative density. The SPS method can generate denser pellets and provide relatively higher Li ionic conductivity compared to other methods. However, it is a low yield and time consuming method.

Table 5. Relative density and ionic conductivity of LLZO electrolytes synthesized with the spark plasma sintering (SPS) method.

Chemical Composition	Sintering Temperature (°C)	Sintering Duration (Hours)	Total Li Ionic Conductivity (mS/cm) at (Temperature)	Relative Density in %	Reference
$Li_{7-x}La_3Zr_{1.5}Ta_{0.5}O_{12}$	1100	50	1.35 (25 °C)	-	[133]
$Li_{3x}La_{2/3-3x}TiO_3$	1100	39	1.00 (22 °C)	100	[121]
$Li_{3x}La_{2/3-3x}TiO_3$	1050	40	5.8×10^{-3} (RT)	98.5	[134]

5. Li Ion Diffusion Mechanism

The tetragonal structure of LLZO has an ordered geometry in which all the sites, tetrahedral 8a, octahedral 16f and octahedral 32g, are fully occupied but the tetrahedral 16e sites are empty [38,40]. Tetragonal LLZO shows good stability at room temperature. On the other hand, the cubic structure possesses disordered geometry because of partially filled tetrahedral 24d and octahedral 96h sites. These partially occupied sites allow Li ions to migrate from one site to another empty site while maintaining the cubic structure even at high temperature [39].

As the Li arrangement in the tetragonal and cubic LLZO is responsible for Li migration, many studies have been performed to reveal the diffusion mechanism of Li. According to Awaka et al. as shown in Figure 3b for cubic LLZO, the tetrahedral 24d sites are almost full whereas the octahedral 96h sites have empty spaces available. As a consequence Li ions move to their neighboring empty positions and form a loop structure as shown in Figure 10 [39].

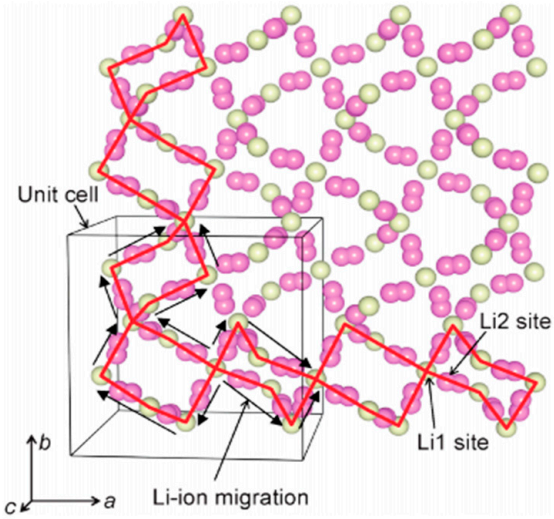

Figure 10. Li ion arrangement in cubic LLZO and loop structure created by migration pathways (reprinted from [39]).

Zhang et al. also proposed the similar migration pattern of Li ions in cubic LLZO, the migration of Li ions from a octahedral site (LiO_6) to adjacent tetrahedral site (LiO_4) and then to another adjacent octahedral site (LiO_6) [135]. They also reported a bottleneck size of Li and O for Li ion migration, and suggested that the bottleneck size of Li-O can be adjusted by proper elemental doping which will allow the Li ions to migrate from the octahedral site to tetrahedral site due to reduced activation energy [135]. Wu et al. reported two possible migration pathways for Ga doped LLZO: (1) the Li ions jump from tetrahedral site 24d to tetrahedral site 24d; however, this pathway is very unlikely because the jump is limited by the migration pathway from tetrahedral site 24d to octahedral site 96h then to tetrahedral site 24d (24d $\rightarrow$ 96h $\rightarrow$ 24d), and (2) Li ions jump from octahedral site 96h to octahedral site 96h (96h $\rightarrow$ 96h); jumping through this pathways occurs at a much higher rate [136].

Meier et al. performed a first principles-based simulation that refuted the assumption made by Awaka and Bernstein on Li site occupancy for cubic LLZO as shown in Figure 5 [41]. Through metadynamics simulation, Meier et al. found that in a tetragonal structure the Li ions are in an ordered arrangement and as a result their motion mechanism are synchronized to each other, i.e., the migration of Li ions are collective in nature; a group of Li ions make the movement at the same time to change their positions as shown in Figure 11a, where activation energy needed for migration is 0.44 eV [41]. But in cubic LLZO the migration of Li ions is not synchronous in nature, and can be treated as a single-ion jump. The arrangements of Li ions in cubic LLZO are not in ordered fashion due to site vacancies, thus triggering a single-ion jump occurs at lower energies, around 0.23 eV, as shown in Figure 11b [41]. According to Meier et al., in cubic LLZO the migration of Li from face sharing tetrahedral site to octahedral site or vice versa (24d $\rightarrow$ 96h/96h $\rightarrow$ 24d) can occur concomitantly at lower potential in comparison to edge sharing octahedral sites (96h $\rightarrow$ 96h) because of the smaller distance.

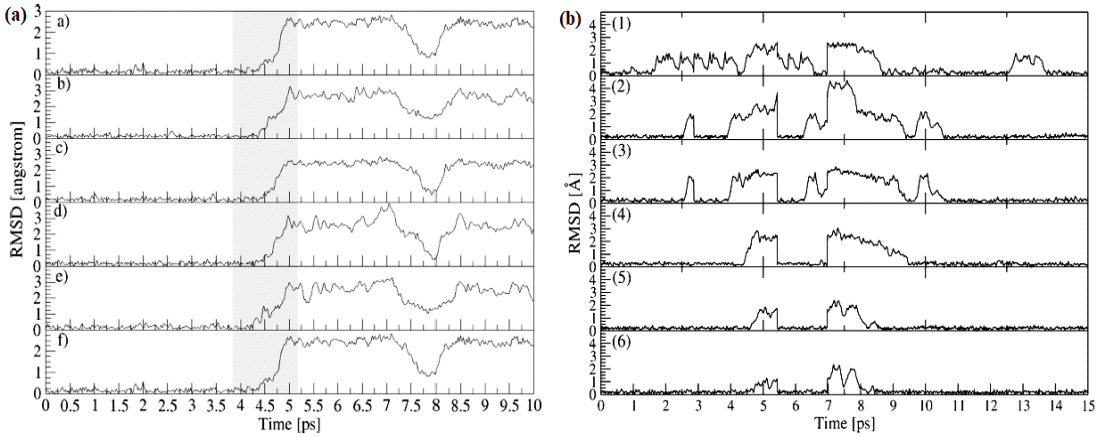

Figure 11. Metadynamics simulation results showing root mean square deviation (RMSD) of 6 individual Li ions at 300 K in (**a**) tetragonal LLZO and (**b**) cubic LLZO. (reprinted from [41]).

6. Doping and Li Ionic Conductivity

After the first report of LLZO by Murugan et al., researchers have tried to find ways to stabilize the cubic LLZO and increase the ionic conductivity of LLZO operating at room temperature [36]. Researchers state similar positions regarding the effects of elemental doping, that it not only stabilizes the cubic phase of LLZO but also improves the ionic conductivity. The cell size of cubic LLZO can shrink or enlarge due to added dopants. This means dopants are responsible for the increased migration of Li ions from one site to another causing the higher ionic conductivity. Also, the concentration of the Li can be adjusted by elemental doping which produces a more disordered lattice arrangement that helps to stabilize the structure at room temperature [137].

In LLZO, 3 sites of Li^+, La^{3+} and Zr^{4+} can be doped using three types of dopant: subvalent, isovalent and supervalent dopants. Many investigations have been performed to find suitable dopant(s) for the suitable site(s) which can produce stable cubic LLZO with a high ionic conductivity [47,55,123,138,139]. Studies show that Al and Ga can give the best results when they are substituted on Li site [47,140–142]. Researchers have made efforts in revealing the effects of changing Li ion concentration on the stability and ionic conductivity by adjusting the number of lithium ions in per formula unit (pfu) [36,59,99,100,104,108,143–145]. The highest Li ionic conductivity was found for Li in the range of 6–7 pfu using supervalent dopants [37,88,137,145].Using low energy potential, an impressive first principles-based study was performed by Miara et al.; they summarized the stability of LLZO when a specific site of the LLZO is doped with different elements in the periodic table. The results are shown in Figure 12 [146], and the total ionic conductivity and activation energy for different cation doping at Li, La and Zr sites are summarized in Table 6.

Bernstein et al. used supervalent Al^{3+} and Ga^{3+} cations into dope Li sites, and found that there is a critical concentration, x = 0.2 pfu for $Li_{7-2x}M_xLa_3Zr_2O_{12}$ (here M = Al and Ga), after this concentration a stable cubic structure is possible [40]. Rangasamy et al. reported an experiment where they used Ce^{4+} as a dopant into La sites and found a stabilized structure with the highest ionic conductivity of 1.4×10^{-5} S/cm for 0.2 pfu of Ce; but the ionic conductivity starts to decrease when Ce content exceeded 0.2 pfu [92]. Doping of the Zr site still is a source of interest as Zr is a common element of Li garnets [16,147,148], so it is possible to explore new information using Zr substitutes; a lot of research has been carried out by doping Zr sites with different cation dopants such as Ta [43,83,149–156], Y [108], Mo [157], Sb [86,99], Nb [158,159], W [79] and Ge [160]. Besides the single site doping, extensive research is also in progress on co-doping of LLZO, in which two or three sites are doped simultaneously to produce a stable structure, however poor ionic conductivity at room temperature is a major concern for co-doping [91,161].

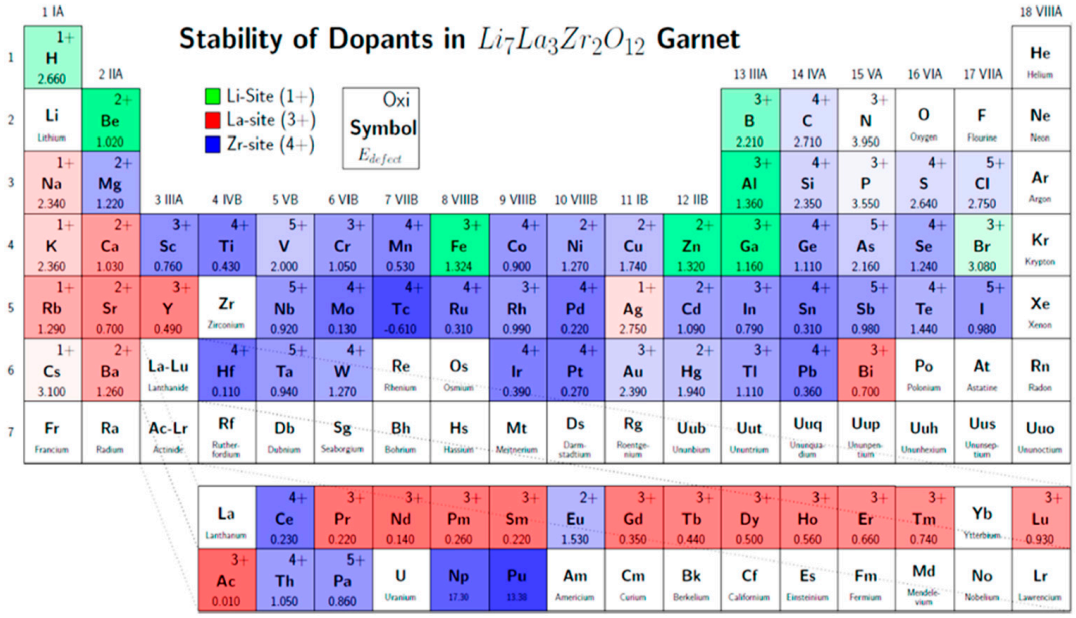

Figure 12. Preferred sites and oxidation states with defect energy (eV) are shown for individual studied dopant element of periodic table. Green, red and blue boxes represent the most stable sites in LLZO for the substitution Li, La and Zr, respectively. (reprinted from [146]).

Table 6. Ionic conductivity and activation energy reported by different groups for single and co-doping with different cation dopants.

Chemical Composition	Total Ionic Conductivity, σ_{total} (mS/cm)	Activation Energy, E_a (eV)	Reference
Li site substitution			
$Li_{6.28}Al_{0.24}La_3Zr_2O_{12}$	0.44 (30 °C)	0.37	[82]
$Li_{6.22}Al_{0.26}La_3Zr_2O_{12}$	0.01 (25 °C)	0.40	[84]
$Li_{6.25}Ga_{0.25}La_3Zr_2O_{12}$	1.46 (RT)	0.25	[76]
$Li_{6.4}Fe_{0.2}La_3Zr_2O_{12}$	1.10 (RT)	-	[75]
$Li_{6.4}Al_{0.05}Ga_{0.15}La_3Zr_2O_{12}$	0.88	0.26	[162]
La site substitution			
$Li_{6.6}La_{2.6}Ce_{0.4}Zr_2O_{12}$	0.01 (RT)	0.48	[92]
$Li_7Nd_3Zr_2O_{12}$	-	0.66	[94]
Sr doped LLZO	0.50 (25 °C)	0.31	[51]
Zr site substitution			
$Li_6La_3ZrTaO_{12}$	0.18 (25 °C)	0.42	[110]
$Li_{6.75}La_3Zr_{1.75}Nb_{0.25}O_{12}$	0.80 (25 °C)	0.31	[109]
$Li_{6.5}La_3Nb_{1.25}Y_{0.75}O_{12}$	0.27 (25 °C) (Bulk)	0.36	[163]
$Li_{6.75}La_3Zr_{1.875}Te_{0.125}O_{12}$	0.33 (30 °C)	0.41	[98]
$Li_{6.55}La_3Hf_{1.55}Ta_{0.45}O_{12}$	0.35 (22 °C)	0.44	[145]
$Li_{6.6}La_3Zr_{1.6}Sb_{0.4}O_{12}$	0.77 (30 °C)	0.34	[99]
$Li_{6.7}La_3Zr_{1.7}Ta_{0.3}O_{12}$	0.69 (RT)	0.36	[105]
$Li_{6.4}La_3Zr_{1.6}W_{0.3}O_{12}$	0.79 (30 °C)	0.45	[100]
$Li_{6.5}La_3Ta_{1.25}Y_{0.75}O_{12}$	0.18 (23 °C)	0.36	[88]
$Li_{6.5}La_3Zr_{1.75}W_{0.25}O_{12}$	0.49 (25 °C)	0.42	[79]
Co-doping: substitution to two or more sites			
$Li_{6.6}La_{2.5}Y_{0.5}Zr_{1.6}Ta_{0.4}O_{12}$	0.23 (27 °C)	0.39	[164]
$Li_6BaLa_2Ta_2O_{12}$	0.09 (50 °C)	0.42	[115]
$Li_6Ba_{0.5}Sr_{0.5}La_2Ta_2O_{12}$	7.1×10^{-3} (18 °C)	0.45	[91]
$Li_6Sr_{0.5}Ca_{0.5}La_2Ta_2O_{12}$	3.2×10^{-3} (18 °C)	0.50	[91]
$Li_{6.5}La_{2.5}Ba_{0.5}ZrTaO_{12}$	0.09 (24 °C)	0.57	[107]

Elemental doping significantly helps to stabilize the structure and transform the phase from tetragonal to cubic. Mori et al. prepared pellets of $Li_{6.25+x}Ga_{0.25}La_{3-x}Sr_xZr_2O_{12}$ that contain different pfu values of Sr content as shown in Figure 13, and found that the pellets at x = 0.1 pfu exhibit good stability and an ionic conductivity as high as 1.3×10^{-3} S/cm with activation energy of 0.25 eV [50]. From the observation of alternating current (AC) impedance spectroscopy as shown in Figure 13a, they found that in the x = 0.0–0.15 pfu range cubic phase GaSr-LLZO with higher ionic conductivity was formed because of the low impedances at the grain-boundary and electrode interface; but with further increasing Sr content, the intercept of the semicircle also increases as shown in Figure 13b. Figure 13c shows the ionic conductivity observed for various Sr composition of x = 0.0–0.5 [50]. Similar results were reported by other groups [52,76,165–167]. It was else reported that the thickness of the pellet might affect the value of conductivity, causing the ionic conductivity to vary for the samples which are even the same in composition and crystal structure [36,168].

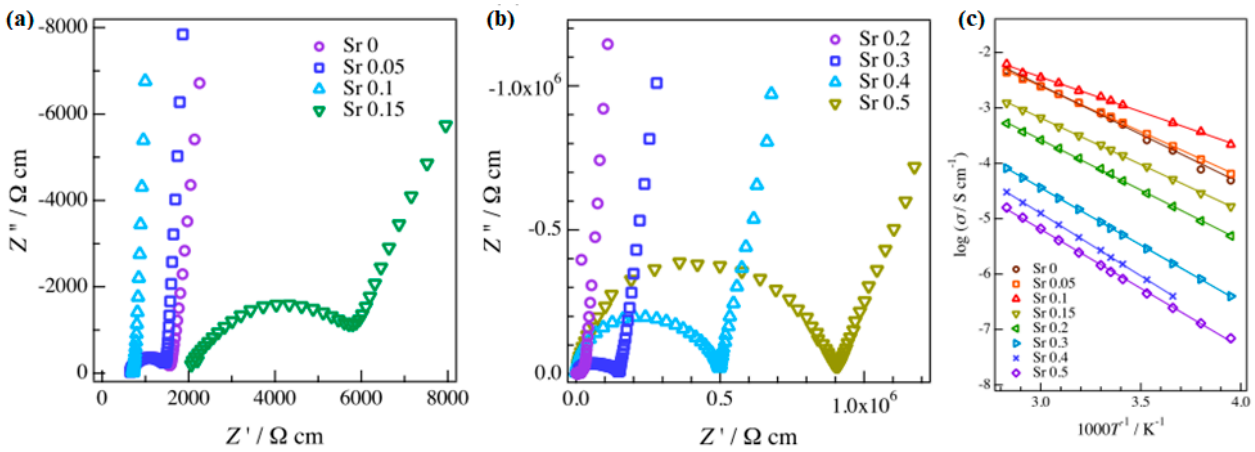

Figure 13. Alternating current (AC) impedance plots of $Li_{6.25+x}Ga_{0.25}La_{3-x}Sr_xZr_2O_{12}$ at 25 °C when (**a**) x = 0–0.15 pfu and (**b**) x = 0.2–0.5 pfu. (**c**) is the Arrhenius plot for x = 0–0.5 showing the dependence of total conductivity vs. inverse temperature (reprinted from [50]).

Recently, Wu et al. performed a comparative study of the change in ionic conductivity and phase transformation of Ga doped $Li_{7-3x}Ga_xLa_3Zr_2O_{12}$ [76]. Based on the XRD patterns and Raman spectra shown in Figure 14, they reported that, for the Ga content, when x < 0.2 pfu the samples exhibited tetragonal phase structure with lower conductivity and higher activation energy; but for $x \geq 0.2$ pfu the samples presented cubic nature with higher ionic conductivity and lower barrier potential [76]. They also reported that the La site can be doped by a Rb cation, yielding cubic LLZO with a high ionic conductivity of 1.62 mS/cm at room temperature; it was attributed to large ionic radius of Rb compared to La, thus facilitating more free space for the migration pathways of Li [138].

Generally, in the sintering process, alumina and platinum crucibles are used which affect the final phase of the sample [138]. Geiger et al. prepared LLZO samples at high temperature using an alumina crucible and found stabilized high conductive cubic phase. This was because at high temperature some the Al from the crucible substituted Li and increased the Li vacancy which helps to stabilize the geometry and increases the mobility of Li ions responsible for conductivity. However, when they used a platinum crucible in sintering, they found that the samples were tetragonal phase [43]. Kumazaki et al. reported that Al from a crucible and Si from the pulverized bowl may reduce the grain-boundary resistance and thus increase the Li ionic conductivity to 6.8×10^{-4} S/cm [122]. However, Xia et al. stated that Al-doped LLZO pellets sintered using a platinum crucible gave better stability, higher Li ionic conductivity and lower grain-boundary resistance because of an increased relative density in contrast to the pellets sintered using a alumina crucible [169]. Liu et al. mentioned that the use of an alumina crucible acted to introduce impure phases

in the sample [54]. In 2009, Awaka et al. successfully prepared transparent tetragonal phase single crystal LLZO by using a gold crucible [38].

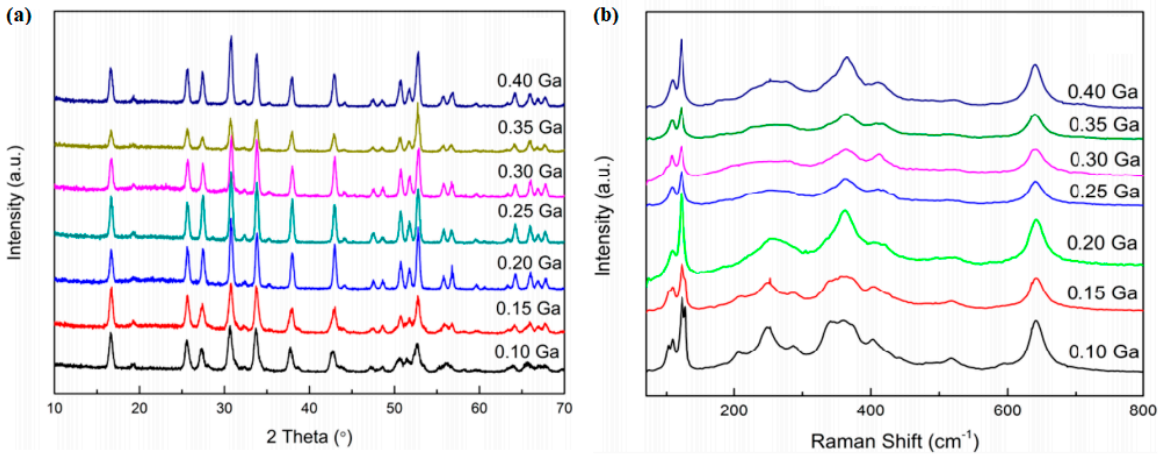

Figure 14. (**a**) X-ray diffraction (XRD) patterns and (**b**) Raman spectra of LLZO doped with Ga at different levels. (reprinted from [76]).

7. Conclusions

Cubic-phase LLZO has proved to be a preferred solid electrolyte because of its high ionic conductivity, low electronic conductivity, wide electrochemical voltage window, good chemical stability with metal Li electrode, and high yield productivity. Intensive research on LLZO is going on to address challenging issues and make the material a practically feasible solid electrolyte for applications in renewable energy storage, electric vehicles, laptops, phones, battery operated electronic devices, etc.

The widely accepted understandings about LLZO solid electrolyte include: (1) LLZO has two structural phases: tetragonal structure ($I4_1/acd$) and cubic structure ($Ia\bar{3}d$); the former is stable at room temperature but exhibits relatively low ionic conductivity, while the latter is stable at high temperatures and shows significantly higher ionic conductivity than the tetragonal phase; (2) in the tetragonal phase, Li ions fully occupy tetrahedral 8a sites and octahedral 16f + 32g sites; but in cubic phase Li ions partially occupy tetrahedral 24d sites and octahedral 96h sites and, at higher temperatures, a transformed cubic phase can be achieved from the tetragonal phase; (3) using a proper sintering technique, it is possible to make denser pellets with a higher conductivity at room temperature due to reduction of grain-boundary resistance; (4) Li ions migrate from the original site to the neighboring site (24d to 96h to 24d) and jump from 96h to 96h; and (5) proper doping can stabilize the cubic structure and increase the ionic conductivity. However, there are some debates regarding the crystal structure and the fabrication of LLZO, involving: (1) the occupancy of Li atoms in tetrahedral 24d and octahedral 96h sites of cubic LLZO; (2) the Li–Li distances in tetragonal and cubic LLZO; (3) the influence of crucibles during high-temperature sintering; and (4) the methods and approaches used to prepare cubic LLZO in the cases of different types of dopant.

Overall, the major challenges in the LLZO research are: (1) to solve chemical instability problem arising from the electrolyte–electrode interface reaction; and (2) find proper composition with elemental cation doping that can result in a higher Li ionic conductivity and can maintain a wide electrochemical voltage window and good chemical stability.

Author Contributions: Conceptualization, Q.Z., M.M.R. and F.A.; writing—original draft preparation, M.M.R.; writing—review and editing, M.J.; supervision, Q.Z.; project administration, Q.Z. and D.W.; funding acquisition, Q.Z. All authors have read and agreed to the published version of the manuscript.

Funding: This project was supported in part by the Department of Energy Grant No. DE-SC0001717 (through the Center for Computationally Assisted Science and Technology (CCAST) at North Dakota State University, of which Prof. Philip Boudjouk is the Principal Investigator) and the National Science Foundation under Grant No. S&CC-1737538.

Institutional Review Board Statement: Not applicable.

Informed Consent Statement: Not applicable.

Data Availability Statement: Data available in a publicly accessible repository.

Acknowledgments: The authors would like to acknowledge financial support from the ND EPSCoR STEM grants program and the North Dakota State University RCA Research Support Services Award.

Conflicts of Interest: The authors declare no conflict of interest.

References

1. Etacheri, V.; Marom, R.; Elazari, R.; Salitra, G.; Aurbach, D. Challenges in the development of advanced Li-ion batteries: A review. *Energy Environ. Sci.* **2011**, *4*, 3243–3262. [CrossRef]
2. Tarascon, J.-M.; Armand, M. Issues and challenges facing rechargeable lithium batteries. *Mater. Sustain. Energy* **2010**, 171–179. [CrossRef]
3. Scrosati, B.; Hassoun, J.; Sun, Y.-K. Lithium-ion batteries. A look into the future. *Energy Environ. Sci.* **2011**, *4*, 3287–3295. [CrossRef]
4. Sloop, S.E.; Pugh, J.K.; Wang, S.; Kerr, J.B.; Kinoshita, K. Chemical Reactivity of PF_5 and $LiPF_6$ in Ethylene Carbonate/Dimethyl Carbonate Solutions. *Electrochem. Solid-State Lett.* **2001**, *4*, A42–A44. [CrossRef]
5. Song, J.; Wang, Y.; Wan, C. Review of gel-type polymer electrolytes for lithium-ion batteries. *J. Power Sources* **1999**, *77*, 183–197. [CrossRef]
6. Vashishta, P.; Mundy, J.N. *Fast Ion Transport in Solids: Electrodes and Electrolytes*; Elsevier North Holland Inc.: Amsterdam, The Netherlands, 1979.
7. Gray, F.M. *Solid Polymer Electrolytes-Fundamentals and Technological Applications*; VCH: New York, NY, USA, 1991.
8. Rogers, R.D. Chemistry: Ionic Liquids—Solvents of the Future? *Science* **2003**, *302*, 792–793. [CrossRef]
9. Gabriel, S.; Weiner, J. Ueber einige Abkömmlinge des Propylamins. *Eur. J. Inorg. Chem.* **1888**, *21*, 2669–2679. [CrossRef]
10. Sato, T.; Maruo, T.; Marukane, S.; Takagi, K. Ionic liquids containing carbonate solvent as electrolytes for lithium ion cells. *J. Power Sources* **2004**, *138*, 253–261. [CrossRef]
11. Gregory, D.H.; O'Meara, P.M.; Gordon, A.G.; Hodges, J.P.; Short, S.; Jorgensen, J.D. Structure of Lithium Nitride and Transition-Metal-Doped Derivatives, Li3-x-yMxN (M = Ni, Cu): A Powder Neutron Diffraction Study. *Chem. Mater.* **2002**, *14*, 2063–2070. [CrossRef]
12. Zintl, E.; Schneider, A. Röntgenanalyse der Lithium-Zink-Legierungen (15. Mitteilung über Metalle und Legierungen). *Z. Elektrochem. Angew. Phys. Chem.* **1935**, *41*, 764–767. [CrossRef]
13. Alpen, U.V.; Rabenau, A.; Talat, G.H. Ionic conductivity in Li3N single crystals. *Appl. Phys. Lett.* **1977**, *30*, 621–623. [CrossRef]
14. Kanno, R.; Murayama, M. Lithium Ionic Conductor Thio-LISICON: The Li_2S-GeS_2-P_2S_5 System. *J. Electrochem. Soc.* **2001**, *148*, A742–A746. [CrossRef]
15. Abrahams, I.; Bruce, P.; West, A.; David, W. Structure determination of LISICON solid solutions by powder neutron diffraction. *J. Solid State Chem.* **1988**, *75*, 390–396. [CrossRef]
16. Bruce, P.; West, A. Ionic conductivity of LISICON solid solutions, $Li_{2+2x}Zn_{1-x}GeO_4$. *J. Solid State Chem.* **1982**, *44*, 354–365. [CrossRef]
17. Von Alpen, U.; Bell, M.F.; Höfer, H.H. Ionic conductivity in $Na_4ZrSi_3O_{10}$. *Solid State Ionics* **1982**, *7*, 345–348. [CrossRef]
18. Hong, H.-P. Crystal structures and crystal chemistry in the system $Na_{1+x}Zr_2Si_xP_{3-x}O_{12}$. *Mater. Res. Bull.* **1976**, *11*, 173–182. [CrossRef]
19. Golub, A.; Shumilova, I.; Zubavichus, Y.; Slovokhotov, Y.; Novikov, Y.; Marie, A.; Danot, M. From single-layer dispersions of molybdenum disulfide towards ternary metal sulfides: Incorporating copper and silver into a MoS_2 matrix. *Solid State Ionics* **1999**, *122*, 137–144. [CrossRef]
20. Aono, H.; Sugimoto, E.; Sadaoka, Y.; Imanaka, N.; Adachi, G. ChemInform Abstract: The Electrical Properties of Ceramic Electrolytes for $LiM_xTi_{2-x}(PO_4)_3$ + yLi_2O, M: Ge, Sn, Hf, and Zr Systems. *J. Electrochem. Soc.* **1993**, *140*, 1827. [CrossRef]
21. Ivanov-Schitz, A. Ionic conductivity of the $NaZr_2(PO_4)_3$ single crystals. *Solid State Ionics* **1997**, *100*, 153–155. [CrossRef]
22. Knauth, P. Inorganic solid Li ion conductors: An overview. *Solid State Ionics* **2009**, *180*, 911–916. [CrossRef]
23. Alamo, J.; Roy, R. Crystal chemistry of the $NaZr_2(PO_4)_3$, NZP or CTP, structure family. *J. Mater. Sci.* **1986**, *21*, 444–450. [CrossRef]
24. Goodenough, J.B.; Hong, H.-P.; Kafalas, J. Fast Na^+-ion transport in skeleton structures. *Mater. Res. Bull.* **1976**, *11*, 203–220. [CrossRef]
25. Sudworth, J. The sodium/sulphur battery. *J. Power Sources* **1984**, *11*, 143–154. [CrossRef]
26. Beevers, C.A.; Ross, M.A.S. The Crystal Structure of "Beta Alumina" $Na_2O{\cdot}11Al_2O_3$. *Z. Krist. Cryst. Mater.* **1937**, *97*, 59–66. [CrossRef]

27. Farrington, G.; Dunn, B.; Briant, J. Li^+ and divalent ion conductivity in beta and beta" alumina. *Solid State Ionics* **1981**, *3–4*, 405–408. [CrossRef]
28. Bettman, M.; Peters, C.R. Crystal structure of $Na_2O.MgO.5Al_2O_3$ [sodium oxide-magnesia-alumina] with reference to $Na_2O.5Al_2O_3$ and other isotypal compounds. *J. Phys. Chem.* **1969**, *73*, 1774–1780. [CrossRef]
29. Bragg, W.L.; Gottfried, C.; West, J. The Structure of β Alumina. *Z. Krist. Cryst. Mater.* **1931**, *77*, 255–274. [CrossRef]
30. Wolfenstine, J.; Allen, J.; Sumner, J.; Sakamoto, J. Electrical and mechanical properties of hot-pressed versus sintered $LiTi_2(PO_4)_3$. *Solid State Ionics* **2009**, *180*, 961–967. [CrossRef]
31. Wang, B.; Chakoumakos, B.C.; Sales, B.; Kwak, B.; Bates, J. Synthesis, Crystal Structure, and Ionic Conductivity of a Polycrystalline Lithium Phosphorus Oxynitride with the γ-Li_3PO_4 Structure. *J. Solid State Chem.* **1995**, *115*, 313–323. [CrossRef]
32. Bates, J.B.; Dudney, N.J.; Neudecker, B.; Ueda, A.; Evans, C.D. Thin-film lithium and lithium-ion batteries. *Solid State Ionics* **2000**, *135*, 33–45. [CrossRef]
33. Catti, M. Local structure of the $Li_{1/8}La_{5/8}TiO_3$(LLTO) ionic conductor by theoretical simulations. *J. Phys. Conf. Ser.* **2008**, *117*, 12008. [CrossRef]
34. Harada, Y.; Ishigaki, T.; Kawai, H.; Kuwano, J. Lithium ion conductivity of polycrystalline perovskite $La_{0.67â^'x}Li_{3x}TiO_3$ with ordered and disordered arrangements of the A-site ions. *Solid State Ionics* **1998**, *108*, 407–413. [CrossRef]
35. Thangadurai, V.; Kaack, H.; Weppner, W.J.F. Novel Fast Lithium Ion Conduction in Garnet-Type $Li_5La_3M_2O_{12}$(M = Nb, Ta). *J. Am. Ceram. Soc.* **2003**, *86*, 437–440. [CrossRef]
36. Murugan, R.; Thangadurai, V.; Weppner, W. Fast Lithium Ion Conduction in Garnet-Type $Li_7La_3Zr_2O_{12}$. *Angew. Chem. Int. Ed.* **2007**, *46*, 7778–7781. [CrossRef] [PubMed]
37. Ramakumar, S.; Janani, N.; Murugan, R. Influence of lithium concentration on the structure and Li^+ transport properties of cubic phase lithium garnets. *Dalton Trans.* **2014**, *44*, 539–552. [CrossRef]
38. Awaka, J.; Kijima, N.; Hayakawa, H.; Akimoto, J. Synthesis and structure analysis of tetragonal $Li_7La_3Zr_2O_{12}$ with the garnet-related type structure. *J. Solid State Chem.* **2009**, *182*, 2046–2052. [CrossRef]
39. Awaka, J.; Takashima, A.; Kataoka, K.; Kijima, N.; Idemoto, Y.; Akimoto, J. Crystal Structure of Fast Lithium-ion-conducting Cubic $Li_7La_3Zr_2O_{12}$. *Chem. Lett.* **2011**, *40*, 60–62. [CrossRef]
40. Bernstein, N.; Johannes, M.D.; Hoang, K. Origin of the Structural Phase Transition in$Li_7La_3Zr_2O_{12}$. *Phys. Rev. Lett.* **2012**, *109*, 205702. [CrossRef]
41. Meier, K.; Laino, T.; Curioni, A. Solid-State Electrolytes: Revealing the Mechanisms of Li-Ion Conduction in Tetragonal and Cubic LLZO by First-Principles Calculations. *J. Phys. Chem. C* **2014**, *118*, 6668–6679. [CrossRef]
42. Kühne, T.D.; Iannuzzi, M.; Del Ben, M.; Rybkin, V.V.; Seewald, P.; Stein, F.; Laino, T.; Khaliullin, R.Z.; Schütt, O.; Schiffmann, F.; et al. CP2K: An electronic structure and molecular dynamics software package—Quickstep: Efficient and accurate electronic structure calculations. *J. Chem. Phys.* **2020**, *152*, 194103. [CrossRef]
43. Geiger, C.A.; Alekseev, E.; Lazic, B.; Fisch, M.; Armbruster, T.; Langner, R.; Fechtelkord, M.; Kim, N.; Pettke, T.; Weppner, W. Crystal Chemistry and Stability of "$Li_7La_3Zr_2O_{12}$" Garnet: A Fast Lithium-Ion Conductor. *Inorg. Chem.* **2011**, *50*, 1089–1097. [CrossRef]
44. Klenk, M.J.; Lai, W. Finite-size effects on the molecular dynamics simulation of fast-ion conductors: A case study of lithium garnet oxide $Li_7La_3Zr_2O_{12}$. *Solid State Ionics* **2016**, *289*, 143–149. [CrossRef]
45. Kuhn, A.; Narayanan, S.; Spencer, L.; Goward, G.; Thangadurai, V.; Wilkening, M. Li self-diffusion in garnet-type $Li_7La_3Zr_2O_{12}$ as probed directly by diffusion-inducedLi7spin-lattice relaxation NMR spectroscopy. *Phys. Rev. B* **2011**, *83*, 094302. [CrossRef]
46. Klenk, M.; Lai, W. Local structure and dynamics of lithium garnet ionic conductors: Tetragonal and cubic $Li_7La_3Zr_2O_7$. *Phys. Chem. Chem. Phys.* **2015**, *17*, 8758–8768. [CrossRef] [PubMed]
47. Buschmann, H.; Dölle, J.; Berendts, S.; Kuhn, A.; Bottke, P.; Wilkening, M.; Heitjans, P.; Senyshyn, A.; Ehrenberg, H.; Lotnyk, A.; et al. Structure and dynamics of the fast lithium ion conductor "$Li_7La_3Zr_2O_{12}$". *Phys. Chem. Chem. Phys.* **2011**, *13*, 19378–19392. [CrossRef] [PubMed]
48. Adams, S.; Rao, R.P. Ion transport and phase transition in $Li_{7-x}La_3(Zr_{2-x}M_x)O_{12}$(M = Ta^{5+}, Nb^{5+}, x = 0, 0.25). *J. Mater. Chem.* **2012**, *22*, 1426–1434. [CrossRef]
49. Cao, S.; Song, S.; Xiang, X.; Hu, Q.; Zhang, C.; Xia, Z.; Xu, Y.; Zha, W.; Li, J.; Gonzale, P.M.; et al. Modeling, Preparation, and Elemental Doping of $Li_7La_3Zr_2O_{12}$ Garnet-Type Solid Electrolytes: A Review. *J. Korean Ceram. Soc.* **2019**, *56*, 111–129. [CrossRef]
50. Mori, D.; Sugimoto, K.; Matsuda, Y.; Ohmori, K.; Katsumata, T.; Taminato, S.; Takeda, Y.; Yamamoto, O.; Imanishi, N. Synthesis, Structure and Ionic Conductivity of Garnet Like Lithium Ion Conductor $Li_{6.25+x}Ga_{0.25}La_{3-x}Sr_xZr_2O_{12}$. *J. Electrochem. Soc.* **2018**, *166*, A5168–A5173. [CrossRef]
51. Dumon, A.; Huang, M.; Shen, Y.; Nan, C.-W. High Li ion conductivity in strontium doped $Li_7La_3Zr_2O_{12}$ garnet. *Solid State Ionics* **2013**, *243*, 36–41. [CrossRef]
52. Matsui, M.; Sakamoto, K.; Takahashi, K.; Hirano, A.; Takeda, Y.; Yamamoto, O.; Imanishi, N. Phase transformation of the garnet structured lithium ion conductor: $Li_7La_3Zr_2O_{12}$. *Solid State Ionics* **2014**, *262*, 155–159. [CrossRef]
53. O'Callaghan, M.P.; Lynham, D.R.; Cussen, E.J.; Chen, G. Structure and Ionic-Transport Properties of Lithium-Containing Garnets $Li_3Ln_3Te_2O_{12}$(Ln = Y, Pr, Nd, Sm−Lu). *Chem. Mater.* **2006**, *18*, 4681–4689. [CrossRef]
54. Liu, K.; Ma, J.-T.; Wang, C.-A. Excess lithium salt functions more than compensating for lithium loss when synthesizing $Li_{6.5}La_3Ta_{0.5}Zr_{1.5}O_{12}$ in alumina crucible. *J. Power Sources* **2014**, *260*, 109–114. [CrossRef]

55. Rangasamy, E.; Wolfenstine, J.; Sakamoto, J. The role of Al and Li concentration on the formation of cubic garnet solid electrolyte of nominal composition $Li_7La_3Zr_2O_{12}$. *Solid State Ionics* **2012**, *206*, 28–32. [CrossRef]
56. Yoo, A.R.; A Yoon, S.; Kim, Y.S.; Sakamoto, J.; Lee, H.C. A Comparative Study on the Synthesis of Al-Doped $Li_{6.2}La_3Zr_2O_{12}$ Powder as a Solid Electrolyte Using Sol–Gel Synthesis and Solid-State Processing. *J. Nanosci. Nanotechnol.* **2016**, *16*, 11662–11668. [CrossRef]
57. Gao, Y.; Wang, X.; Wang, W.; Fang, Q. Sol–gel synthesis and electrical properties of $Li_5La_3Ta_2O_{12}$ lithium ionic conductors. *Solid State Ionics* **2010**, *181*, 33–36. [CrossRef]
58. Kokal, I.; Somer, M.; Notten, P.; Hintzen, H. Sol–gel synthesis and lithium ion conductivity of $Li_7La_3Zr_2O_{12}$ with garnet-related type structure. *Solid State Ionics* **2011**, *185*, 42–46. [CrossRef]
59. Shimonishi, Y.; Toda, A.; Zhang, T.; Hirano, A.; Imanishi, N.; Yamamoto, O.; Takeda, Y. Synthesis of garnet-type $Li_{7-x}La_3Zr_2O_{12-1/2x}$ and its stability in aqueous solutions. *Solid State Ionics* **2011**, *183*, 48–53. [CrossRef]
60. Xie, H.; Li, Y.; Goodenough, J.B. Low-temperature synthesis of $Li_7La_3Zr_2O_{12}$ with cubic garnet-type structure. *Mater. Res. Bull.* **2012**, *47*, 1229–1232. [CrossRef]
61. Janani, N.; Deviannapoorani, C.; Dhivya, L.; Murugan, R. Influence of sintering additives on densification and Li^+ conductivity of Al doped $Li_7La_3Zr_2O_{12}$ lithium garnet. *RSC Adv.* **2014**, *4*, 51228–51238. [CrossRef]
62. Gao, Y.; Wang, X.; Wang, W.; Zhuang, Z.; Zhang, D.; Fang, Q. Synthesis, ionic conductivity, and chemical compatibility of garnet-like lithium ionic conductor $Li_5La_3Bi_2O_{12}$. *Solid State Ionics* **2010**, *181*, 1415–1419. [CrossRef]
63. Jin, Y.; McGinn, P.J. Al-doped $Li_7La_3Zr_2O_{12}$ synthesized by a polymerized complex method. *J. Power Sources* **2011**, *196*, 8683–8687. [CrossRef]
64. Lobe, S.; Dellen, C.; Finsterbusch, M.; Gehrke, H.-G.; Sebold, D.; Tsai, C.-L.; Uhlenbruck, S.; Guillon, O. Radio frequency magnetron sputtering of $Li_7La_3Zr_2O_{12}$ thin films for solid-state batteries. *J. Power Sources* **2016**, *307*, 684–689. [CrossRef]
65. Kalita, D.; Lee, S.; Lee, K.; Ko, D.; Yoon, Y. Ionic conductivity properties of amorphous Li–La–Zr–O solid electrolyte for thin film batteries. *Solid State Ionics* **2012**, *229*, 14–19. [CrossRef]
66. Park, J.S.; Cheng, L.; Zorba, V.; Mehta, A.; Cabana, J.; Chen, G.; Doeff, M.M.; Richardson, T.J.; Park, J.H.; Son, J.-W.; et al. Effects of crystallinity and impurities on the electrical conductivity of Li–La–Zr–O thin films. *Thin Solid Films* **2015**, *576*, 55–60. [CrossRef]
67. Tan, J.; Tiwari, A. Fabrication and Characterization of $Li_7La_3Zr_2O_{12}$ Thin Films for Lithium Ion Battery. *ECS Solid State Lett.* **2012**, *1*, Q57–Q60. [CrossRef]
68. Kim, S.; Hirayama, M.; Taminato, S.; Kanno, R. Epitaxial growth and lithium ion conductivity of lithium-oxide garnet for an all solid-state battery electrolyte. *Dalton Trans.* **2013**, *42*, 13112–13117. [CrossRef] [PubMed]
69. Afyon, S.; Krumeich, F.; Rupp, J.L.M. A shortcut to garnet-type fast Li-ion conductors for all-solid state batteries. *J. Mater. Chem. A* **2015**, *3*, 18636–18648. [CrossRef]
70. Dhivya, L.; Karthik, K.; Ramakumar, S.; Murugan, R. Facile synthesis of high lithium ion conductive cubic phase lithium garnets for electrochemical energy storage devices. *RSC Adv.* **2015**, *5*, 96042–96051. [CrossRef]
71. Chen, R.-J.; Huang, M.; Huang, W.-Z.; Shen, Y.; Lin, Y.-H.; Nan, C.-W. Sol–gel derived Li–La–Zr–O thin films as solid electrolytes for lithium-ion batteries. *J. Mater. Chem. A* **2014**, *2*, 13277–13282. [CrossRef]
72. Quinlan, F.T.; Vidu, R.; Predoana, L.; Zaharescu, M.; Gartrner, M.; Groza, J.; Stroeve, P. Lithium Cobalt Oxide ($LiCoO_2$) Nanocoatings by Sol−Gel Methods. *Ind. Eng. Chem. Res.* **2004**, *43*, 2468–2477. [CrossRef]
73. Yi, E.; Wang, W.; Kieffer, J.; Laine, R.M. Flame made nanoparticles permit processing of dense, flexible, Li^+ conducting ceramic electrolyte thin films of cubic-$Li_7La_3Zr_2O_{12}$ (c-LLZO). *J. Mater. Chem. A* **2016**, *4*, 12947–12954. [CrossRef]
74. Gai, J.; Zhao, E.; Ma, F.; Sun, D.; Ma, X.; Jin, Y.; Wu, Q.; Cui, Y. Improving the Li-ion conductivity and air stability of cubic $Li_7La_3Zr_2O_{12}$ by the co-doping of Nb, Y on the Zr site. *J. Eur. Ceram. Soc.* **2018**, *38*, 1673–1678. [CrossRef]
75. Rettenwander, D.; Wagner, R.; Reyer, A.; Bonta, M.; Cheng, L.; Doeff, M.M.; Limbeck, A.; Wilkening, M.; Amthauer, G. Interface Instability of Fe-Stabilized $Li_7La_3Zr_2O_{12}$ versus Li Metal. *J. Phys. Chem. C* **2018**, *122*, 3780–3785. [CrossRef]
76. Wu, J.-F.; Chen, E.-Y.; Yu, Y.; Liu, L.; Wu, Y.; Pang, W.K.; Peterson, V.K.; Guo, X. Gallium-Doped $Li_7La_3Zr_2O_{12}$ Garnet-Type Electrolytes with High Lithium-Ion Conductivity. *ACS Appl. Mater. Interfaces* **2017**, *9*, 1542–1552. [CrossRef]
77. Tong, X.; Thangadurai, V.; Wachsman, E.D. Highly Conductive Li Garnets by a Multielement Doping Strategy. *Inorg. Chem.* **2015**, *54*, 3600–3607. [CrossRef]
78. Liu, C.; Wen, Z.Y.; Rui, K. High Ion conductivity in garnet-type F-doped $Li_7La_3Zr_2O_{12}$. *Wuji Cailiao Xuebao J. Inorgnanic Materails* **2015**. [CrossRef]
79. Li, Y.; Wang, Z.; Cao, Y.; Du, F.; Chen, C.; Cui, Z.; Guo, X. W-Doped $Li_7La_3Zr_2O_{12}$ Ceramic Electrolytes for Solid State Li-ion Batteries. *Electrochimica Acta* **2015**, *180*, 37–42. [CrossRef]
80. Narayanan, S.; Ramezanipour, F.; Thangadurai, V. Dopant Concentration–Porosity–Li-Ion Conductivity Relationship in Garnet-Type $Li_{5+2x}La3Ta_{2-x}Y_xO_{12}$ ($0.05 \leq x \leq 0.75$) and Their Stability in Water and 1 M LiCl. *Inorg. Chem.* **2015**, *54*, 6968–6977. [CrossRef] [PubMed]
81. Nemori, H.; Matsuda, Y.; Mitsuoka, S.; Matsui, M.; Yamamoto, O.; Takeda, Y.; Imanishi, N. Stability of garnet-type solid electrolyte $LixLa3A_{2-y}B_yO_{12}$ (A=Nb or Ta, B=Sc or Zr). *Solid State Ionics* **2015**, *282*, 7–12. [CrossRef]
82. Deviannapoorani, C.; Ramakumar, S.; Janani, N.; Murugan, R. Synthesis of lithium garnets from $La_2Zr_2O_7$ pyrochlore. *Solid State Ionics* **2015**, *283*, 123–130. [CrossRef]

83. Janani, N.; Ramakumar, S.; Kannan, S.; Murugan, R. Optimization of Lithium Content and Sintering Aid for Maximized Li^+ Conductivity and Density in Ta-Doped Li_7 La_3 Zr_2 O_{12}. *J. Am. Ceram. Soc.* **2015**, *98*, 2039–2046. [CrossRef]
84. Wang, D.; Zhong, G.; Pang, W.K.; Guo, Z.; Li, Y.; McDonald, M.J.; Fu, R.; Mi, J.-X.; Yang, Y. Toward Understanding the Lithium Transport Mechanism in Garnet-type Solid Electrolytes: Li^+ Ion Exchanges and Their Mobility at Octahedral/Tetrahedral Sites. *Chem. Mater.* **2015**, *27*, 6650–6659. [CrossRef]
85. Inada, R.; Kusakabe, K.; Tanaka, T.; Kudo, S.; Sakurai, Y. Synthesis and properties of Al-free $Li_{7-x}La_3Zr_{2-x}Ta_xO_{12}$ garnet related oxides. *Solid State Ionics* **2014**, *262*, 568–572. [CrossRef]
86. Cao, Z.-Z.; Ren, W.; Liu, J.-R.; Li, G.-R.; Gao, Y.-F.; Fang, M.-H.; He, W.-Y. Microstructure and Ionic Conductivity of Sb-doped $Li_7La_3Zr_2O_{12}$ Ceramics. *J. Inorg. Mater.* **2014**, *29*, 220–224. [CrossRef]
87. Nemori, H.; Matsuda, Y.; Matsui, M.; Yamamoto, O.; Takeda, Y.; Imanishi, N. Relationship between lithium content and ionic conductivity in the $Li_{5+2x}La_3Nb_{2-x}Sc_xO_{12}$ system. *Solid State Ionics* **2014**, *266*, 9–12. [CrossRef]
88. Baral, A.K.; Narayanan, S.; Ramezanipour, F.; Thangadurai, V. Evaluation of fundamental transport properties of Li-excess garnet-type $Li_{5+2x}La_3Ta_{2-x}Y_xO_{12}$ (x = 0.25, 0.5 and 0.75) electrolytes using AC impedance and dielectric spectroscopy. *Phys. Chem. Chem. Phys.* **2014**, *16*, 11356–11365. [CrossRef]
89. Li, Y.; Wang, Z.; Li, C.; Cao, Y.; Guo, X. Densification and ionic-conduction improvement of lithium garnet solid electrolytes by flowing oxygen sintering. *J. Power Sources* **2014**, *248*, 642–646. [CrossRef]
90. Wang, D.; Zhong, G.; Dolotko, O.; Li, Y.; McDonald, M.J.; Mi, J.; Fu, R.; Yang, Y. The synergistic effects of Al and Te on the structure and Li^+-mobility of garnet-type solid electrolytes. *J. Mater. Chem. A* **2014**, *2*, 20271–20279. [CrossRef]
91. Zeier, W.G.; Zhou, S.; López-Bermúdez, B.; Page, K.; Melot, B.C. Dependence of the Li-Ion Conductivity and Activation Energies on the Crystal Structure and Ionic Radii in $Li_6MLa_2Ta_2O_{12}$. *ACS Appl. Mater. Interfaces* **2014**, *6*, 10900–10907. [CrossRef]
92. Rangasamy, E.; Wolfenstine, J.; Allen, J.; Sakamoto, J. The effect of 24c-site (A) cation substitution on the tetragonal–cubic phase transition in $Li_{7-x}La_{3-x}A_xZr_2O_{12}$ garnet-based ceramic electrolyte. *J. Power Sources* **2013**, *230*, 261–266. [CrossRef]
93. Hitz, G.T.; Wachsman, E.D.; Thangadurai, V. Highly Li-Stuffed Garnet-Type $Li_{7+x}La_3Zr_{2-x}Y_xO_{12}$. *J. Electrochem. Soc.* **2013**, *160*, A1248–A1255. [CrossRef]
94. Howard, M.A.; Clemens, O.; Knight, K.S.; Anderson, P.A.; Hafiz, S.; Panchmatia, P.M.; Slater, P.R. Synthesis, conductivity and structural aspects of $Nd_3Zr_2Li_{7-3x}Al_xO_{12}$. *J. Mater. Chem. A* **2013**, *1*, 14013. [CrossRef]
95. Truong, L.; Colter, J.; Thangadurai, V. Chemical stability of Li-stuffed garnet-type $Li_{5+x}Ba_xLa_{3-x}Ta_2O_{12}$ (x = 0, 0.5, 1) in water: A comparative analysis with the Nb analogue. *Solid State Ionics* **2013**, *247–248*, 1–7. [CrossRef]
96. Mariappan, C.R.; Gnanasekar, K.I.; Jayaraman, V.; Gnanasekaran, T. Lithium ion conduction in $Li_5La_3Ta_2O_{12}$ and $Li_7La_3Ta_2O_{13}$ garnet-type materials. *J. Electroceramics* **2013**, *30*, 258–265. [CrossRef]
97. Li, Y.; Cao, Y.; Guo, X. Influence of lithium oxide additives on densification and ionic conductivity of garnet-type $Li_{6.75}La_3Zr_{1.75}Ta_{0.25}O_{12}$ solid electrolytes. *Solid State Ionics* **2013**, *253*, 76–80. [CrossRef]
98. Deviannapoorani, C.; Dhivya, L.; Ramakumar, S.; Murugan, R. Lithium ion transport properties of high conductive tellurium substituted $Li_7La_3Zr_2O_{12}$ cubic lithium garnets. *J. Power Sources* **2013**, *240*, 18–25. [CrossRef]
99. Ramakumar, S.; Satyanarayana, L.; Manorama, S.V.; Murugan, R. Structure and Li^+ dynamics of Sb-doped $Li_7La_3Zr_2O_{12}$ fast lithium ion conductors. *Phys. Chem. Chem. Phys.* **2013**, *15*, 11327. [CrossRef]
100. Dhivya, L.; Janani, N.; Palanivel, B.; Murugan, R. Li^+ transport properties of W substituted $Li_7La_3Zr_2O_{12}$ cubic lithium garnets. *AIP Adv.* **2013**, *3*, 082115. [CrossRef]
101. Buschmann, H.; Berendts, S.; Mogwitz, B.; Janek, J. Lithium metal electrode kinetics and ionic conductivity of the solid lithium ion conductors "$Li_7La_3Zr_2O_{12}$" and $Li_{7-x}La_3Zr_{2-x}Ta_xO_{12}$ with garnet-type structure. *J. Power Sources* **2012**, *206*, 236–244. [CrossRef]
102. Il'Ina, E.; Andreev, O.; Antonov, B.; Batalov, N. Morphology and transport properties of the solid electrolyte $Li_7La_3Zr_2O_{12}$ prepared by the solid-state and citrate–nitrate methods. *J. Power Sources* **2012**, *201*, 169–173. [CrossRef]
103. Tan, J.; Tiwari, A. Synthesis of Cubic Phase $Li_7La_3Zr_2O_{12}$ Electrolyte for Solid-State Lithium-Ion Batteries. *Electrochem. Solid-State Lett.* **2012**, *15*, A37. [CrossRef]
104. Huang, M.; Dumon, A.; Nan, C.-W. Effect of Si, In and Ge doping on high ionic conductivity of $Li_7La_3Zr_2O_{12}$. *Electrochem. Commun.* **2012**, *21*, 62–64. [CrossRef]
105. Wang, Y.; Lai, W. High Ionic Conductivity Lithium Garnet Oxides of $Li_{7-x}La_3Zr_{2-x}Ta_xO_{12}$ Compositions. *Electrochem. Solid-State Lett.* **2012**, *15*, A68–A71. [CrossRef]
106. Li, Y.; Han, J.-T.; Wang, C.-A.; Xie, H.; Goodenough, J.B. Optimizing Li^+ conductivity in a garnet framework. *J. Mater. Chem.* **2012**, *22*, 15357–15361. [CrossRef]
107. Narayanan, S.; Epp, V.; Wilkening, M.; Thangadurai, V. Macroscopic and microscopic Li^+ transport parameters in cubic garnet-type "$Li_{6.5}La_{2.5}Ba_{0.5}ZrTaO_{12}$" as probed by impedance spectroscopy and NMR. *RSC Adv.* **2012**, *2*, 2553–2561. [CrossRef]
108. Murugan, R.; Ramakumar, S.; Janani, N. High conductive yttrium doped $Li_7La_3Zr_2O_{12}$ cubic lithium garnet. *Electrochem. Commun.* **2011**, *13*, 1373–1375. [CrossRef]
109. Ohta, S.; Kobayashi, T.; Asaoka, T. High lithium ionic conductivity in the garnet-type oxide Li_{7-X} $La_3(Zr_{2-X}, Nb_X)O_{12}$ (X = 0–2). *J. Power Sources* **2011**, *196*, 3342–3345. [CrossRef]
110. Li, Y.; Wang, C.-A.; Xie, H.; Cheng, J.; Goodenough, J.B. High lithium ion conduction in garnet-type $Li_6La_3ZrTaO_{12}$. *Electrochem. Commun.* **2011**, *13*, 1289–1292. [CrossRef]

111. Kotobuki, M.; Munakata, H.; Kanamura, K.; Sato, Y.; Yoshida, T. Compatibility of $Li_7La_3Zr_2O_{12}$ Solid Electrolyte to All-Solid-State Battery Using Li Metal Anode. *J. Electrochem. Soc.* **2010**, *157*, A1076. [CrossRef]
112. Zaiß, T.; Ortner, M.; Murugan, R.; Weppner, W. Fast ionic conduction in cubic hafnium garnet $Li_7La_3Hf_2O_{12}$. *Ionics* **2010**, *16*, 855–858. [CrossRef]
113. Awaka, J.; Kijima, N.; Kataoka, K.; Hayakawa, H.; Ohshima, K.-I.; Akimoto, J. Neutron powder diffraction study of tetragonal $Li_7La_3Hf_2O_{12}$ with the garnet-related type structure. *J. Solid State Chem.* **2010**, *183*, 180–185. [CrossRef]
114. Wang, W.; Wang, X.; Gao, Y.; Fang, Q. Lithium-ionic diffusion and electrical conduction in the $Li_7La_3Ta_2O_{13}$ compounds. *Solid State Ionics* **2009**, *180*, 1252–1256. [CrossRef]
115. Murugan, R.; Thangadurai, V.; Weppner, W. Effect of lithium ion content on the lithium ion conductivity of the garnet-like structure $Li_{5+x}BaLa_2Ta_2O_{11.5+0.5x}$ (x = 0–2). *Appl. Phys. A* **2008**, *91*, 615–620. [CrossRef]
116. Lee, C.-H.; Park, G.-J.; Choi, J.; Doh, C.-H.; Bae, D.-S.; Kim, J.-S.; Lee, S.-M. Low temperature synthesis of garnet type solid electrolyte by modified polymer complex process and its characterization. *Mater. Res. Bull.* **2016**, *83*, 309–315. [CrossRef]
117. Sakamoto, J.; Rangasamy, E.; Kim, H.; Kim, Y.; Wolfenstine, J. Synthesis of nano-scale fast ion conducting cubic $Li_7La_3Zr_2O_{12}$. *Nanotechnology* **2013**, *24*, 424005. [CrossRef] [PubMed]
118. Raskovalov, A.; Il'Ina, E.; Antonov, B. Structure and transport properties of $Li_7La_3Zr_{2-0.75x}Al_xO_{12}$ superionic solid electrolytes. *J. Power Sources* **2013**, *238*, 48–52. [CrossRef]
119. Janani, N.; Ramakumar, S.; Dhivya, L.; Deviannapoorani, C.; Saranya, K.; Murugan, R. Synthesis of cubic $Li_7La_3Zr_2O_{12}$ by modified sol–gel process. *Ionics* **2011**, *17*, 575–580. [CrossRef]
120. Zhang, Y.; Chen, F.; Tu, R.; Shen, Q.; Zhang, L. Field assisted sintering of dense Al-substituted cubic phase $Li_7La_3Zr_2O_{12}$ solid electrolytes. *J. Power Sources* **2014**, *268*, 960–964. [CrossRef]
121. Kobayashi, Y.; Miyashiro, H.; Takeuchi, T.; Shigemura, H.; Balakrishnan, N.; Tabuchi, M.; Kageyama, H.; Iwahori, T. All-solid-state lithium secondary battery with ceramic/polymer composite electrolyte. *Solid State Ionics* **2002**, *152–153*, 137–142. [CrossRef]
122. Kumazaki, S.; Iriyama, Y.; Kim, K.-H.; Murugan, R.; Tanabe, K.; Yamamoto, K.; Hirayama, T.; Ogumi, Z. High lithium ion conductive $Li_7La_3Zr_2O_{12}$ by inclusion of both Al and Si. *Electrochem. Commun.* **2011**, *13*, 509–512. [CrossRef]
123. Li, Y.; Han, J.; Wang, C.-A.; Vogel, S.C.; Xie, H.; Xu, M.; Goodenough, J.B. Ionic distribution and conductivity in lithium garnet $Li_7La_3Zr_2O_{12}$. *J. Power Sources* **2012**, *209*, 278–281. [CrossRef]
124. Cao, Y.; Li, Y.-Q.; Guo, X.-X.; Yang, C.; Yi-Qiu, L.; Xiang-Xin, G. Densification and lithium ion conductivity of garnet-type $Li_{7-x}La_3Zr_{2-x}Ta_xO_{12}$(x= 0.25) solid electrolytes. *Chin. Phys. B* **2013**, *22*, 078201. [CrossRef]
125. Rosenkiewitz, N.; Schuhmacher, J.; Bockmeyer, M.; Deubener, J. Nitrogen-free sol–gel synthesis of Al-substituted cubic garnet $Li_7La_3Zr_2O_{12}$ (LLZO). *J. Power Sources* **2015**, *278*, 104–108. [CrossRef]
126. Takano, R.; Tadanaga, K.; Hayashi, A.; Tatsumisago, M. Low temperature synthesis of Al-doped $Li_7La_3Zr_2O_{12}$ solid electrolyte by a sol–gel process. *Solid State Ionics* **2014**, *255*, 104–107. [CrossRef]
127. Suzuki, Y.; Kami, K.; Watanabe, K.; Saito, N.; Ohnishi, T.; Takada, K.; Sudo, R.; Imanishi, N. Transparent cubic garnet-type solid electrolyte of Al_2O_3-doped $Li_7La_3Zr_2O_{12}$. *Solid State Ionics* **2015**, *278*, 172–176. [CrossRef]
128. Qin, S.; Zhu, X.; Jiang, Y.; Ling, M.; Hu, Z.; Zhu, J. Extremely dense microstructure and enhanced ionic conductivity in hot-isostatic pressing treated cubic garnet-type solid electrolyte of Ga_2O_3-doped $Li_7La_3Zr_2O_{12}$. *Funct. Mater. Lett.* **2018**, *11*, 1850029. [CrossRef]
129. Wolfenstine, J.; Sakamoto, J.; Allen, J.L. Electron microscopy characterization of hot-pressed Al substituted $Li_7La_3Zr_2O_{12}$. *J. Mater. Sci.* **2012**, *47*, 4428–4431. [CrossRef]
130. Wolfenstine, J.; Ratchford, J.; Rangasamy, E.; Sakamoto, J.; Allen, J.L. Synthesis and high Li-ion conductivity of Ga-stabilized cubic $Li_7La_3Zr_2O_{12}$. *Mater. Chem. Phys.* **2012**, *134*, 571–575. [CrossRef]
131. Zhang, Y.; Cai, J.; Chen, F.; Tu, R.; Shen, Q.; Zhang, X.; Zhang, L. Preparation of cubic $Li_7La_3Zr_2O_{12}$ solid electrolyte using a nano-sized core–shell structured precursor. *J. Alloy. Compd.* **2015**, *644*, 793–798. [CrossRef]
132. Botros, M.; Djenadic, R.; Clemens, O.; Möller, M.; Hahn, H. Field assisted sintering of fine-grained $Li_{7-3}La_3Zr_2Al\ O_{12}$ solid electrolyte and the influence of the microstructure on the electrochemical performance. *J. Power Sources* **2016**, *309*, 108–115. [CrossRef]
133. Baek, S.-W.; Lee, J.-M.; Kim, T.Y.; Song, M.-S.; Park, Y. Garnet related lithium ion conductor processed by spark plasma sintering for all solid state batteries. *J. Power Sources* **2014**, *249*, 197–206. [CrossRef]
134. Mei, A.; Jiang, Q.-H.; Lin, Y.-H.; Nan, C.-W. Lithium lanthanum titanium oxide solid-state electrolyte by spark plasma sintering. *J. Alloy. Compd.* **2009**, *486*, 871–875. [CrossRef]
135. Zhang, Y.; Chen, F.; Li, J.; Zhang, L.; Gu, J.; Zhang, D.; Saito, K.; Guo, Q.; Luo, P.; Dong, S. Regulation mechanism of bottleneck size on Li^+ migration activation energy in garnet-type $Li_7La_3Zr_2O_{12}$. *Electrochim. Acta* **2018**, *261*, 137–142. [CrossRef]
136. Wu, J.-F.; Pang, W.K.; Peterson, V.K.; Wei, L.; Guo, X. Garnet-Type Fast Li-Ion Conductors with High Ionic Conductivities for All-Solid-State Batteries. *ACS Appl. Mater. Interfaces* **2017**, *9*, 12461–12468. [CrossRef] [PubMed]
137. Miara, L.J.; Ong, S.P.; Mo, Y.; Richards, W.D.; Park, Y.; Lee, J.-M.; Lee, H.S.; Ceder, G. Effect of Rb and Ta Doping on the Ionic Conductivity and Stability of the Garnet $Li_{7+2x-y}(La_{3-x}Rb_x)(Zr_{2-y}Tay)O_{12}$ ($0 \leq x \leq 0.375$, $0 \leq y \leq 1$) Superionic Conductor: A First Principles Investigation. *Chem. Mater.* **2013**, *25*, 3048–3055. [CrossRef]
138. Kotobuki, M.; Kanamura, K.; Sato, Y.; Yoshida, T. Fabrication of all-solid-state lithium battery with lithium metal anode using Al_2O_3-added $Li_7La_3Zr_2O_{12}$ solid electrolyte. *J. Power Sources* **2011**, *196*, 7750–7754. [CrossRef]

139. Düvel, A.; Kuhn, A.; Robben, L.; Wilkening, M.; Heitjans, P. Mechanosynthesis of Solid Electrolytes: Preparation, Characterization, and Li Ion Transport Properties of Garnet-Type Al-Doped $Li_7La_3Zr_2O_{12}$ Crystallizing with Cubic Symmetry. *J. Phys. Chem. C* **2012**, *116*, 15192–15202. [CrossRef]
140. Allen, J.; Wolfenstine, J.; Rangasamy, E.; Sakamoto, J. Effect of substitution (Ta, Al, Ga) on the conductivity of $Li_7La_3Zr_2O_{12}$. *J. Power Sources* **2012**, *206*, 315–319. [CrossRef]
141. Rettenwander, D.; Geiger, C.A.; Amthauer, G. Synthesis and Crystal Chemistry of the Fast Li-Ion Conductor $Li_7La_3Zr_2O_{12}$Doped with Fe. *Inorg. Chem.* **2013**, *52*, 8005–8009. [CrossRef]
142. Hubaud, A.A.; Schroeder, D.J.; Key, B.; Ingram, B.J.; Dogan, F.; Vaughey, J.T. Low temperature stabilization of cubic $(Li_{7-x}Al_{x/3})La_3Zr_2O_{12}$: Role of aluminum during formation. *J. Mater. Chem. A* **2013**, *1*, 8813. [CrossRef]
143. Galven, C.; Fourquet, J.-L.; Crosnier-Lopez, M.-P.; Le Berre, F. Instability of the Lithium Garnet $Li_7La_3Sn_2O_{12}$: Li^+/H^+Exchange and Structural Study. *Chem. Mater.* **2011**, *23*, 1892–1900. [CrossRef]
144. Thangadurai, V.; Weppner, W. Investigations on electrical conductivity and chemical compatibility between fast lithium ion conducting garnet-like $Li_6BaLa_2Ta_2O_{12}$ and lithium battery cathodes. *J. Power Sources* **2005**, *142*, 339–344. [CrossRef]
145. Gupta, A.; Murugan, R.; Paranthaman, M.; Bi, Z.; Bridges, C.A.; Nakanishi, M.; Sokolov, A.P.; Han, K.S.; Hagaman, E.; Xie, H.; et al. Optimum lithium-ion conductivity in cubic $Li_{7-x}La_3Hf_{2-x}Ta_xO_{12}$. *J. Power Sources* **2012**, *209*, 184–188. [CrossRef]
146. Miara, L.J.; Richards, W.D.; Wang, Y.; Ceder, G. First-Principles Studies on Cation Dopants and Electrolyte | Cathode Interphases for Lithium Garnets. *Chem. Mater.* **2015**, *27*, 4040–4047. [CrossRef]
147. Alpen, U.V.; Bell, M.F.; Wichelhaus, W.; Cheung, K.Y.; Dudley, G.J. Ionic conductivity of $Li_{14}Zn(GeO_{44}$(Lisicon). *Electrochimica Acta* **1978**, *23*, 1395–1397. [CrossRef]
148. Bruce, P.G.; West, A.R. The A-C Conductivity of Polycrystalline LISICON, Li_{2+2x} Zn_{1-x} GeO_4, and a Model for Intergranular Constriction Resistances. *J. Electrochem. Soc.* **1983**, *130*, 662–669. [CrossRef]
149. Shao, C.; Liu, H.; Yu, Z.; Zheng, Z.; Sun, N.; Diao, C. Structure and ionic conductivity of cubic $Li_7La_3Zr_2O_{12}$ solid electrolyte prepared by chemical co-precipitation method. *Solid State Ionics* **2016**, *287*, 13–16. [CrossRef]
150. Jonson, R.A.; McGinn, P.J. Tape casting and sintering of $Li7La3Zr_{1.75}Nb_{0.25}Al_{0.1}O_{12}$ with Li_3BO_3 additions. *Solid State Ionics* **2018**, *323*, 49–55. [CrossRef]
151. Hayamizu, K.; Matsuda, Y.; Matsui, M.; Imanishi, N. Lithium ion diffusion measurements on a garnet-type solid conductor $Li_{6.6}La_3Zr_{1.6}Ta_{0.4}O_{12}$ by using a pulsed-gradient spin-echo NMR method. *Solid State Nucl. Magn. Reson.* **2015**, *70*, 21–27. [CrossRef]
152. A Yoon, S.; Oh, N.R.; Yoo, A.R.; Lee, H.G. Preparation and Characterization of Ta-substituted $Li_7La_3Zr_{2-x}O_{12}$ Garnet Solid Electrolyte by Sol-Gel Processing. *J. Korean Ceram. Soc.* **2017**, *54*, 278–284. [CrossRef]
153. Cheng, S.H.-S.; He, K.-Q.; Liu, Y.; Zha, J.-W.; Kamruzzaman; Ma, L.W.; Dang, Z.-M.; Li, R.K.; Chung, C. Electrochemical performance of all-solid-state lithium batteries using inorganic lithium garnets particulate reinforced PEO/$LiClO_4$ electrolyte. *Electrochim. Acta* **2017**, *253*, 430–438. [CrossRef]
154. Stanje, B.; Rettenwander, D.; Breuer, S.; Uitz, M.; Berendts, S.; Lerch, M.; Uecker, R.; Redhammer, G.; Hanzu, I.; Wilkening, M. Solid Electrolytes: Extremely Fast Charge Carriers in Garnet-Type $Li_6La_3ZrTaO_{12}$ Single Crystals. *Ann. Phys.* **2017**, *529*, 1700140. [CrossRef]
155. Ren, Y.; Liu, T.; Shen, Y.; Lin, Y.; Nan, C.-W. Garnet-type oxide electrolyte with novel porous-dense bilayer configuration for rechargeable all-solid-state lithium batteries. *Ionics* **2017**, *23*, 2521–2527. [CrossRef]
156. El-Shinawi, H.; Cussen, E.J.; Corr, S.A. Enhancement of the lithium ion conductivity of Ta-doped $Li_7La_3Zr_2O_{12}$ by incorporation of calcium. *Dalton Trans.* **2017**, *46*, 9415–9419. [CrossRef]
157. Liu, X.; Li, Y.; Yang, T.; Cao, Z.; He, W.; Gao, Y. High lithium ionic conductivity in the garnet-type oxide $Li_{7-2x}La_3Zr_{2-x}Mo_xO_{12}$ (x = 0–0.3) ceramics by sol-gel method. *J. Am. Ceram. Soc.* **2017**, *100*, 1527–1533. [CrossRef]
158. Liu, C.; Rui, K.; Shen, C.; Badding, M.E.; Zhang, G.; Wen, Z. Reversible ion exchange and structural stability of garnet-type Nb-doped $Li_7La_3Zr_2O_{12}$ in water for applications in lithium batteries. *J. Power Sources* **2015**, *282*, 286–293. [CrossRef]
159. Tang, Y.; Luo, Z.; Liu, T.; Liu, P.; Li, Z.; Lu, A. Effects of B_2O_3 on microstructure and ionic conductivity of $Li_{6.}5La3Zr_{1.5}Nb_{0.5}O_{12}$ solid electrolyte. *Ceram. Int.* **2017**, *43*, 11879–11884. [CrossRef]
160. Hu, S.; Li, Y.-F.; Yang, R.; Yang, Z.; Wang, L. Structure and ionic conductivity of $Li_7La_3Zr_{2-x}Ge_xO_{12}$ garnet-like solid electrolyte for all solid state lithium ion batteries. *Ceram. Int.* **2018**, *44*, 6614–6618. [CrossRef]
161. Gu, W.; Ezbiri, M.; Rao, R.P.; Avdeev, M.; Adams, S. Effects of penta- and trivalent dopants on structure and conductivity of $Li_7La_3Zr_2O_{12}$. *Solid State Ionics* **2015**, *274*, 100–105. [CrossRef]
162. Rettenwander, D.; Redhammer, G.; Preishuber-Pflügl, F.; Cheng, L.; Miara, L.; Wagner, R.; Welzl, A.; Suard, E.; Doeff, M.; Wilkening, M.; et al. Structural and Electrochemical Consequences of Al and Ga Cosubstitution in $Li_7La_3Zr_2O_{12}$ Solid Electrolytes. *Chem. Mater.* **2016**, *28*, 2384–2392. [CrossRef]
163. Narayanan, S.; Ramezanipour, F.; Thangadurai, V. Enhancing Li Ion Conductivity of Garnet-Type $Li_5La_3Nb_2O_{12}$ by Y^- and Li^-Codoping: Synthesis, Structure, Chemical Stability, and Transport Properties. *J. Phys. Chem. C* **2012**, *116*, 20154–20162. [CrossRef]
164. Dhivya, L.; Murugan, R. Effect of Simultaneous Substitution of Y and Ta on the Stabilization of Cubic Phase, Microstructure, and Li^+ Conductivity of $Li_7La_3Zr_2O_{12}$ Lithium Garnet. *ACS Appl. Mater. Interfaces* **2014**, *6*, 17606–17615. [CrossRef] [PubMed]

165. Wagner, R.; Redhammer, G.J.; Rettenwander, D.; Senyshyn, A.; Schmidt, W.; Wilkening, M.; Amthauer, G. Crystal Structure of Garnet-Related Li-Ion Conductor $Li_{7-3x}Ga_xLa_3Zr_2O_{12}$: Fast Li-Ion Conduction Caused by a Different Cubic Modification? *Chem. Mater.* **2016**, *28*, 1861–1871. [CrossRef] [PubMed]
166. Matsuda, Y.; Itami, Y.; Hayamizu, K.; Ishigaki, T.; Matsui, M.; Takeda, Y.; Yamamoto, O.; Imanishi, N. Phase relation, structure and ionic conductivity of $Li_{7-x-3y}Al_yLa_3Zr_{2-x}Ta_xO_{12}$. *RSC Adv.* **2016**, *6*, 78210–78218. [CrossRef]
167. Matsuda, Y.; Sakaida, A.; Sugimoto, K.; Mori, D.; Takeda, Y.; Yamamoto, O.; Imanishi, N. Sintering behavior and electrochemical properties of garnet-like lithium conductor $Li_{6.25}M_{0.25}La_3Zr_2O_{12}$ (M: Al^{3+} and Ga^{3+}). *Solid State Ionics* **2017**, *311*, 69–74. [CrossRef]
168. Murugan, R.; Thangadurai, V.; Weppner, W. Schnelle Lithiumionenleitung in granatartigem $Li_7La_3Zr_2O_{12}$. *Angew. Chem.* **2007**, *119*, 7925–7928. [CrossRef]
169. Xia, W.; Xu, B.; Duan, H.; Guo, Y.; Kang, H.; Li, H.; Liu, H. Ionic Conductivity and Air Stability of Al-Doped $Li_7La_3Zr_2O_{12}$ Sintered in Alumina and Pt Crucibles. *ACS Appl. Mater. Interfaces* **2016**, *8*, 5335–5342. [CrossRef]